Mon. Not. R. Astron. Soc. **396,** 1895–1914 (2009) doi:10.1111/j.1365-2966.2009.14839.x

Mg and TiO spectral features at the near-IR: spectrophotometric index definitions and empirical calibrations

A. J. Cenarro,[1⋆] N. Cardiel,[2] A. Vazdekis[1] and J. Gorgas[2]

[1] *Instituto de Astrofísica de Canarias, E-38200, La Laguna, Tenerife, Spain*
[2] *Depto. de Astrofísica, Fac. de Ciencias Físicas, Universidad Complutense de Madrid, E-28040 Madrid, Spain*

Accepted 2009 March 26. Received 2009 March 25; in original form 2008 December 4

ABSTRACT

Using the near-infrared spectral stellar library of Cenarro et al., the behaviour of the Mg I line at 8807 Å and nearby TiO bands is analyzed in terms of the effective temperature, surface gravity and metallicity of the library stars. New spectroscopic indices for both spectral features – namely MgI and sTiO – are defined, and their sensitivities to different signal-to-noise ratios, spectral resolutions, flux calibrations and sky emission-line residuals are characterized. The two new indices exhibit interesting properties. In particular, MgI is a good indicator of the Mg abundance, whereas sTiO is a powerful dwarf-to-giant discriminator for cold spectral types. Empirical fitting polynomials that reproduce the strength of the new indices as a function of the stellar atmospheric parameters are computed, and a FORTRAN routine with the fitting function predictions is made available. A thorough study of several error sources, non-solar [Mg/Fe] ratios and their influence on the fitting function residuals is also presented. From this analysis, an [Mg/Fe] underabundance of ~ -0.04 is derived for the Galactic open cluster M67.

Key words: stars: abundances – stars: fundamental parameters – globular clusters: general – galaxies: stellar content.

1 INTRODUCTION

A powerful approach to unravel the stellar content of unresolved stellar systems is to interpret the integrated strengths of key spectral features on the basis of evolutionary stellar population synthesis models (e.g. Worthey 1994; Vazdekis et al. 1996; Vazdekis 1999; Bruzual & Charlot 2003; Thomas, Maraston & Bender 2003; Vazdekis et al. 2003, hereafter VAZ03; Maraston 2005; Schiavon 2007). These models make use of theoretical isochrones and spectral stellar libraries to predict integrated line-strengths and/or spectral energy distributions (SEDs) corresponding to simple stellar populations (SSPs) of a given age, overall metallicity, abundance pattern, initial mass function and star formation history.

Till date, major progress in this kind of studies has been achieved in the optical spectral range. The Lick/IDS (Lick Observatory Image Dissector Scanner) stellar library (Gorgas et al. 1993; Worthey et al. 1994) became the reference system for most optical work on this topic. However, thanks to the developing of much improved optical stellar libraries that supersede the capabilities of the Lick/IDS library, like e.g. Jones (1998), ELODIE (Prugniel & Soubiran 2001, 2004; Prugniel et al. 2007), STELIB (Le Borgne et al. 2003), the Indo–US stellar library (Valdés et al. 2004) and MILES (Medium resolution INT Library of Empirical Spectra) (Sánchez-Blázquez et al. 2006; Cenarro et al. 2007), a new generation of SSP models in the optical region (e.g. Vazdekis 1999; Bruzual & Charlot 2003; PÉGASE-HR, by Le Borgne et al. 2004; Vazdekis et al., in preparation) is now available. The larger spectral coverage and better spectral resolution of the new models have motivated the development of new analysis approaches that, rather than focusing on single spectral features, are based on fitting techniques over the full spectrum that are potentially useful for reconstructing in the first order the star formation histories of galaxies (e.g. Panter, Heavens & Jimenez 2003; Cid Fernandes et al. 2005; Mathis, Charlot & Brinchmann 2006; Ocvirk et al. 2006a,b; Panter et al. 2007; Koleva et al. 2008).

Apart from the above work, there exists an important effort to advance in our understanding of complementary spectral regions which are governed by different types of stars, like the ultraviolet (e.g. Fanelli et al. 1992; Gregg et al. 2004; Heap & Lindler 2007) and the infrared (e.g. Ivanov et al. 2004; Ranade et al. 2004, 2007a,b; Mármol-Queraltó et al. 2008). In particular, aimed at providing reliable SSP model predictions for the near-infrared (near-IR) spectral region around Ca II triplet at ∼8600 Å, an extensive spectral stellar library at λλ 8348–9020 Å [full width at half-maximum (FWHM) =1.5 Å] that comprises 706 stars over a wide range of

⋆E-mail: cenarro@iac.es

atmospheric parameters was developed by Cenarro et al. (2001a, hereafter CEN01a). Subsequent libraries like STELIB and the Indo–US also include the Ca II triplet region. Initially, the library in Cenarro et al. (2001) was particularly devoted to understand the behaviour of the Ca II triplet in individual stars. With this aim, improved line-strength indices for this spectral feature (namely CaT, PaT, CaT*), which are especially suited to be measured in the integrated spectra of stellar populations, were defined (CEN01a). Also, to minimize uncertainties and systematic errors of the empirical calibration of the indices, a homogeneous system of revised atmospheric parameters for the library stars was derived in Cenarro et al. (2001b) (hereafter CEN01b). Putting all these ingredients together, the behaviour of the Ca II indices as a function of the stellar atmospheric parameters was computed by means of so-called empirical fitting functions (FFs; Cenarro et al. 2002, hereafter CEN02), which were implemented into the evolutionary synthesis code of VAZ03 to predict the integrated indices and the near-IR SEDs for SSPs of different ages, metallicities and initial mass function (IMFs).

The present paper can be considered as an extension of the above project to two nearby spectral features: the Mg I line at λ 8807 Å and the molecular bands of TiO at $\lambda\lambda$ 8432, 8442, 8452 Å and $\lambda\lambda$ 8860, 8868 Å. As already shown in Cenarro et al. (2003) for a sample or 35 early-type galaxies, both spectral features – together with the Ca II triplet – can play an important role in characterizing the properties of old and intermediate-aged stellar populations. The fact that Mg is overabundant with respect to Fe in massive elliptical galaxies and tightly correlates with the velocity dispersion (e.g. Dressler et al. 1987; Worthey, Faber & Gonzalez 1992; and others) turns Mg indices into a key element to constrain galaxy star formation and evolution theories. Also, it is worth stressing the importance of calibrating several spectroscopic indicators in relatively narrow spectral regions, as the ages and metallicities derived from a set of nearby indices are expected to be consistent even for composite stellar populations.

Therefore, the main objective of this paper is to carry out a comprehensive study of the Mg I and TiO features in individual stars, so that their dependences with the atmospheric parameters are calibrated and quantified via empirical FFs. A forthcoming paper by Vazdekis et al. (in preparation) will be devoted to present and discuss the corresponding SSP model predictions (both based on such FFs and from the SEDs in VAZ03) in comparison with galactic observational data.

Section 2 is focused on the definition of new line-strength indices for the Mg I line and the TiO bands and on the comparison with those of previous work. The new index sensitivities to different spectral resolutions, signal-to-noise ratios (S/N), flux calibration, reddening uncertainties, and residuals of sky lines and telluric absorptions are analyzed. Also, accurate formulae for estimating random errors in the new index measurements are provided. After a qualitative description of the Mg I line and the TiO band strengths on the basis of the library stars, Section 3 is devoted to the mathematical fitting procedure of the index strengths as functions of the stellar atmospheric parameters, providing the significant terms, coefficients and statistics of the derived FFs. A thorough analysis of the FF residuals and possible error sources is herein presented, accounting for the uncertainties in the input atmospheric parameters, the flux calibration and the effect of different [Mg/Fe] ratios in the Mg I line FFs. A qualitative comparison with MgI and sTiO predictions based on theoretical work is presented in Section 4. To conclude, Section 5 is reserved to discuss and summarize the main contents and results of this paper.

2 MgI AND TiO SPECTROSCOPIC INDICES

Before focusing on the definition of new line-strength indices for the measurement of the Mg I and TiO spectral features, it is worth making a brief description of the spectral range under study. The existence of other absorption lines around the spectral features of interest is indeed decisive for a proper location of the index bandpasses. As in CEN01a, the strongest spectral features around 8600 Å are labelled in Fig. 1 for a subsample of representative spectral types; the Mg I line and TiO bands concerning this paper are indicated in spectra (c) and (d), respectively. It is readily seen from that figure that the H Paschen series completely dominates the spectra of the hottest stars. Its strength decreases with the decreasing temperature whilst several metal lines become stronger. For G, K and early-M spectral types, the spectra are mainly governed by the Ca II triplet, the Mg I line, and many other Fe and Ti absorption lines. Finally, intermediate and late-M types exhibit strong molecular bands of TiO and VO which modulate the shape of the local continuum (see CEN01a and CEN02 for a more detailed description of the above behaviours).

2.1 Previous index definitions

Despite the fact that most previous papers dealing with the present spectral range mainly focused on the Ca II triplet, a few of them considered the Mg I line at 8807 Å and the TiO bands at $\lambda\lambda$ 8432, 8442, 8452 Å and $\lambda\lambda$ 8860, 8868 Å. This was the case of Díaz, Terlevich & Terlevich (1989, hereafter DTT) and Carter, Visvanathan & Pickles (1986, hereafter CVP), who provided index definitions for the Mg I line and the TiO bands, respectively. Table 1 lists the bandpass limits of the corresponding indices as defined in the above papers. In turn, Figs 2 and 3 illustrate the suitability of these indices when measured over different spectral types.

In the 1990s, the indices defined by DTT were the most widely employed to measure the strengths of the Ca II triplet[1] and the Mg I lines. For the Mg I spectral feature, they defined a *classical* atomic index that consists of a central bandpass enclosing the Mg I line, and two continuum bandpasses located at both sides – blue and red – of the central one. In spite of being a well-defined index for F–K spectral types, it suffers from two main limitations: (i) the presence of strong Paschen lines (P11 and P12) in early spectral types makes the derived pseudo-continuum to be unreliable (Fig. 2a), and (ii) the proximity of the red continuum bandpass to the TiO break around 8600 Å makes the index to be very sensitive to spectral resolution and velocity dispersion broadening (Fig. 2c). This is particularly critical for the integrated spectra of galaxies in which TiO bands may be prominent (see e.g. the SEDs predicted in VAZ03), and typical velocity dispersions are above $\sim$100 km s^{-1}. In any case, it is fair noting the intrinsic difficulty of defining an Mg I line-strength index in a spectral region dominated by strong absorption lines. This is particularly evident in the case of the earliest spectral types (see Fig. 2a), for which the Mg I line is very weak and the wings of the Paschen lines are blended, thus decreasing the true continuum level.

The work by CVP defined *classical* molecular indices to measure the strength of the TiO bands. Again, the index consists of two continuum bandpasses and a very wide central bandpass for the TiO break at $\sim$8450 Å (see Table 1). Because of the width of the central bandpass, the index turns out to be sensitive to the Ca II triplet

[1] The suitability of this and other Ca II indices is discussed in CEN01a.

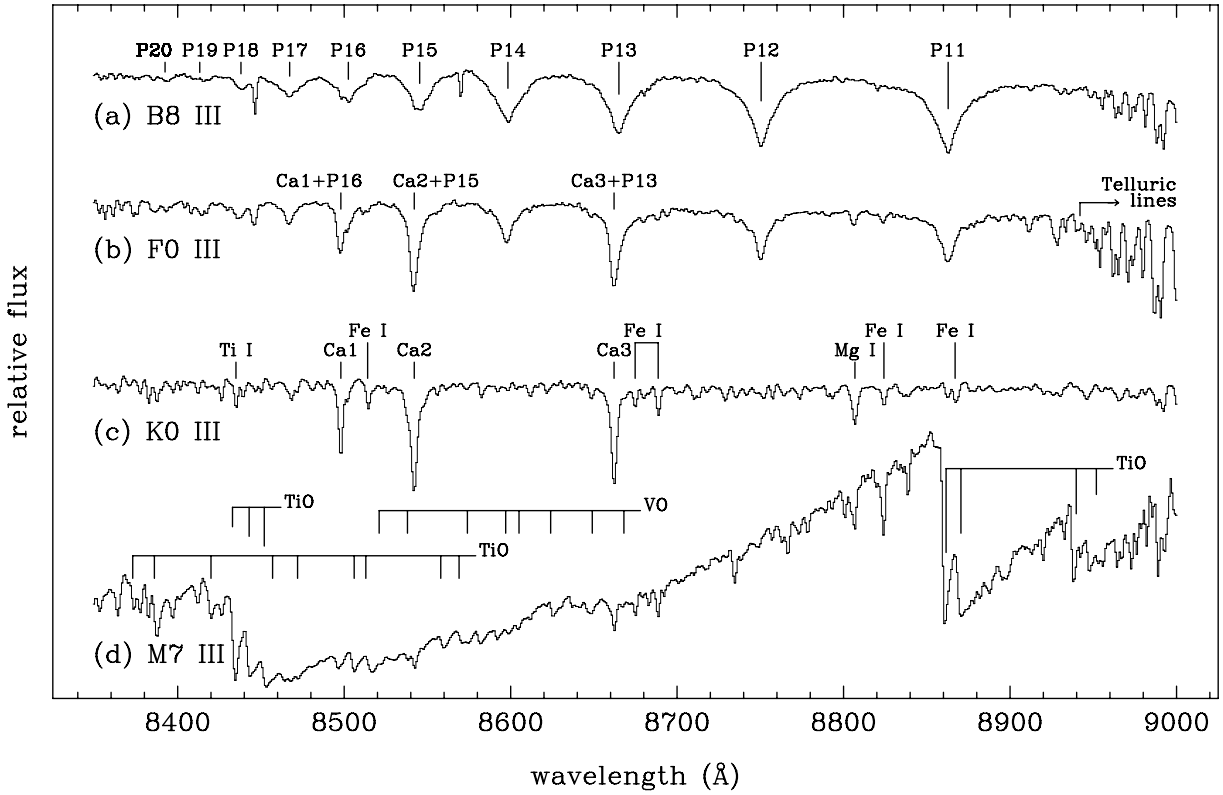

Figure 1. Spectra of the stars HD 186568 (B8 III), HD 89025 (F0 III), HD 216228 (K0 III) and HD 114961 (M7 III) in the spectral range of the stellar library from CEN01a. The strongest features in this region are marked: the Paschen series (from P11 to P20), the Ca II triplet (Ca1, Ca2 and Ca3), several metal lines and telluric absorptions. The Mg I line and the molecular bands of TiO and VO are indicated in spectra (c) and (d), respectively.

Table 1. Definition of previous and new indices for the near-IR Mg I line (λ 8807 Å) and TiO bands (λλ 8432, 8442, 8452 Å; λλ 8860, 8868 Å). Codes for the references are as follow: CVP (Carter et al. 1986), DTT (Díaz et al. 1989), TW (this work). Types *c– a*, *c– m*, *g– a* and *g–s* refer to classical–atomic, classical–molecular, generic–atomic and generic–slope-like indices, respectively.

Index	Type	Central bandpass (Å)	Continuum bandpasses (Å)
MgI (DTT)	*c–a*	8799.5–8814.5	8775.0–8787.0
			8845.0–8855.0
MgI (TW)	*g–a*	8802.5–8811.0	8781.0–8789.0
			8831.0–8835.5
			8841.5–8846.0
TiO_1 (CVP)	*c–m*	8450.0–8700.0	8350.0–8400.0
			8750.0–8800.0
TiO_2 (CVP)	*c–m*	8890.0–9060.0	8790.0–8840.0
			9100.0–9150.0
sTiO (TW)	*g–s*	None	8474.0–8484.0
			8563.0–8577.0
			8619.0–8642.0
			8700.0–8725.0
			8776.0–8792.0

and the Paschen lines for those spectral types in which the above features dominate the spectrum (Figs 3a and b). Such a Ca and H contamination for most spectral types is obviously not desired when trying to understand the behaviour of the TiO bands with the stellar atmospheric parameters, as it would translate into a blurring of age and metallicity effects if the TiO index were used as a tool for stellar population diagnostics.

2.2 New index definitions

In CEN01a, we introduced a new type of line-strength indices, namely *generic* indices, which allow the definition of an arbitrary but precise number of continuum bandpasses to derive the pseudo-continuum level. It is computed as an error-weighted, least-squares linear fit to all the pixels of these continuum bandpasses. Generic indices also allow the inclusion of various bandpasses for adjacent spectral features, which are thus measured simultaneously – using different relative weights – under the same pseudo-continuum. As we report in that paper, the above improvements are highly advantageous in regions densely populated by other spectral features, telluric lines or strong sky emission lines, as is the case for the near-IR spectral range. CaT, PaT and CaT* are examples of generic indices for the Ca II triplet and three lines of the H Paschen series (see details in CEN01a).

The new generic indices that we characterize here, MgI and sTiO, were formerly measured in Cenarro et al. (2003) for a sample of early-type galaxies. We devote the current paper to provide full details on their definition, sensitivities and behaviour with the stellar atmospheric parameters.

2.2.1 The MgI index

The MgI index has been defined as a generic index consisting of three continuum bandpasses and one spectral-feature bandpass for the Mg I line. Fig. 4 illustrates the MgI index defined in this work when measured over the same spectra as in Fig. 2, and the bandpass limits are listed in Table 1. The location and width of these bandpasses were established in order to derive a reliable

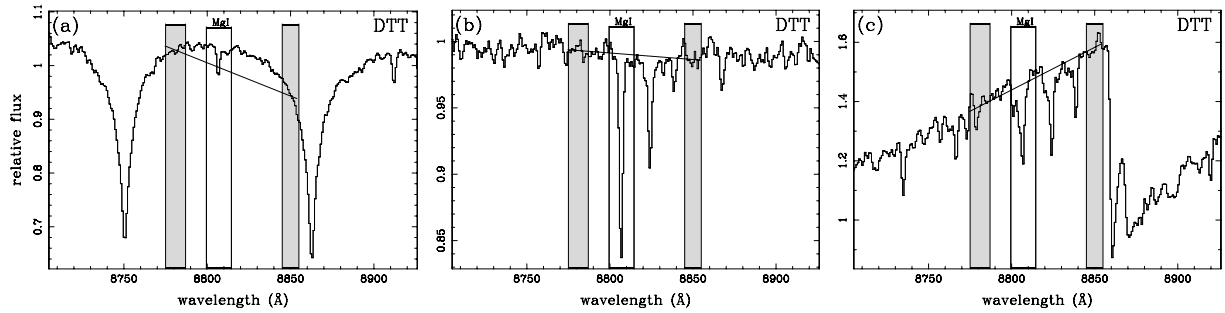

Figure 2. Index definition by DTT for the Mg I line over different spectral types. The spectra, taken from the stellar library of CEN01a, correspond to HD 161817 (A2 VI; *a*), HD 25329 (K1 Vsb; *b*) and HD 148783 (M6 III; *c*). Grey and open bands illustrate, respectively, the location of continuum and central bandpasses (see Table 1). Solid lines represent the local pseudo-continua computed by means of error-weighted least-squares fit to all the pixels in the continuum bandpasses.

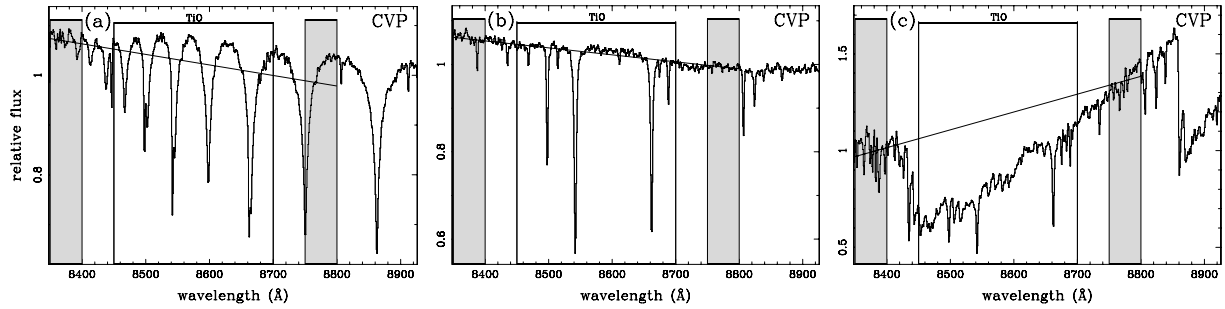

Figure 3. Index definition for the TiO bands by CVP (TiO_1; see Table 1) over different spectral types. Spectra, bandpasses colour code and solid lines are the same as in Fig. 2.

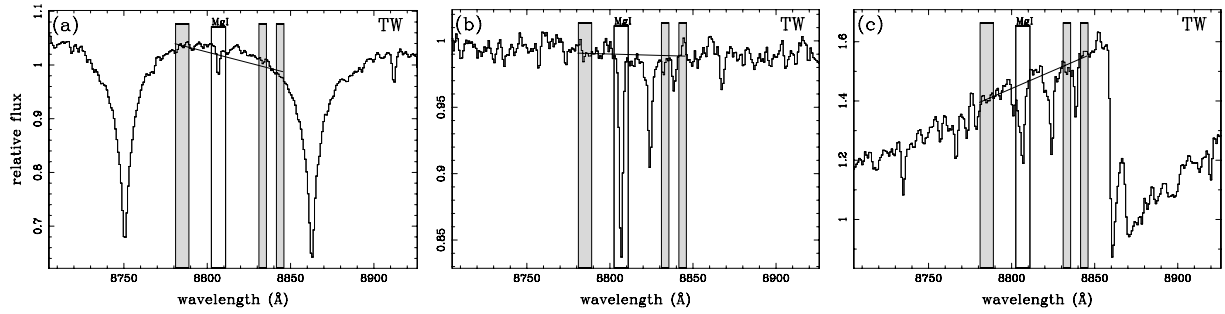

Figure 4. New index definition (this work; TW) for the Mg I line, MgI, over the same spectral types of Fig. 2. Again, grey and open bandpasses illustrate, respectively, the location of continuum and central bandpasses (see Table 1), whilst solid lines represent the local pseudo-continua derived from error-weighted least-squares fit to all the pixels in the continuum bandpasses.

pseudo-continuum for all the spectral types even when the spectra are broadened up to 300 km s^{-1}. Also, since we are interested in measuring MgI on broadened galaxy spectra, we ensured that the TiO break at λ 8860 Å was not affecting the pseudo-continuum level. Note however that because of the problem reported in the previous section the pseudo-continuum derived for early spectral types is still slightly below the true level (Fig. 4a). With the aim of defining a reliable indicator of Mg abundance, we tried to avoid as much as possible the presence of other metal lines within the spectral-feature band (e.g. see Fig. 4c). This is why we preferred to define a quite narrow characteristic bandpass, even though it increases the sensitivity of the index to the spectral resolution. A reasonable compromise between both requirements was finally established.

2.2.2 *The sTiO index*

For the measurement of the TiO bands, we introduce a new type of generic index which will be referred to as *slope* index. Slope indices are defined as the ratio between the pseudo-continuum values at the central wavelengths of any two continuum bandpasses. In this sense, they can be considered as a measurement of the local pseudo-continuum slope. It is important to note that although slope indices just consider the pseudo-continuum values at the centre of two continuum bandpasses the total number of continuum bandpasses driving the pseudo-continuum level can be as large as desired. In practice, one actually performs an error-weighted least-squares linear fit to all the pixels within the full set of considered

continuum bandpasses. After that, the linear fit is evaluated at the central wavelengths of the first and last of those bandpasses.

This new concept of index was conceived with the aim of measuring the slope of the continuum around the Ca II triplet, mainly governed by molecular absorptions (TiO and VO) in mid- and late-M spectral types. Given that the location of the five continuum bandpasses for the indices CaT, PaT or CaT* leads to a reliable pseudo-continuum for all the spectral types (see Figure 5), we took advantage of the previous indices to define the slope index sTiO. In particular, it is defined as the ratio between the pseudo-continuum values, $C(\lambda)$, at the central wavelengths of the reddest and bluest continuum bandpasses (see Table 1), that is

$$\mathrm{sTiO} = \frac{C(\lambda 8784.0)}{C(\lambda 8479.0)}. \quad (1)$$

At variance with other spectrophotometric indices, sTiO is potentially sensitive to flux calibration uncertainties (hence extinction effects) given that its continuum bandpasses spread over more than 300 Å. On the other hand, it is particularly unsensitive to low S/N as the slope gets robustly constrained by five bandpasses that cover overall 88 Å. These and other effects will be discussed in Section 2.4.

2.2.3 *MgI and sTiO measurements for the library stars*

The new indices have been measured for all the spectra in CEN01a at the nominal resolution of the library, that is, FWHM = 1.5 Å or $\sigma = 22.2\,\mathrm{km\ s^{-1}}$. Table 10 lists the index measurements and their errors, which account for the photon noise and radial velocity uncertainties, the latter including typical errors in wavelength calibration. [A sample of Table 10 is included here; the full table is available in the online version of the article (see Supporting Information).] This data base is also available at http://www.ucm.es/info/Astrof/ellipt/MgIsTiO.html.

The actual measurements have been performed with INDEXF (Cardiel 2007), a C++ program specially written to compute atomic, molecular, break, generic-atomic, generic-break and slope indices in wavelength-calibrated FITS spectra. This program is available at http://www.ucm.es/info/Astrof/software/indexf.

2.3 Conversions between the new and previous index systems

For those readers interested in transforming old system data of indices into the new ones (or vice versa), this section provides a set of calibrations to make conversions from one system to the other. Table 2 lists the derived relations and Fig. 6 illustrates the corresponding fits.

Table 2. Calibrations between different index systems. σ_{rms}: unbiased standard deviation of the fit. N: number of stars in the fit. T_{eff} (K): Effective temperature region where the calibration was obtained. These calibrations are graphically displayed in Fig. 6.

Calibrations	σ_{rms}	N	T_{eff} (K)
MgI = 0.119 + 0.864 MgI (DTT)	0.07	560	2750–6300
sTiO = 0.822 + 3.397 $\mathrm{TiO_1}$(CVP)	0.07	29	2750–3700
MgI (DTT) = $\mathrm{MgI\ (DTT)_{DTT}}$	0.16	100	3425–6800

Using the 706 library stars from CEN01a, we have compared the measurements of the indices MgI (DTT) and $\mathrm{TiO_1}$ (CVP) with the ones corresponding to the new MgI and sTiO. The calibrations were computed by means of error-weighted least-squares fit to a straight line that, in both cases, turned out to be statistically significant. The location and width of the MgI (DTT) bandpasses (see Section 2.1) cause hot stars to depart from the general trend of the rest of the library stars (Fig. 6a). The calibration between the TiO indices (Fig. 6b) was derived just considering those stars cold enough to exhibit molecular bands in their spectra. Otherwise, the fit would be strongly dominated by the behaviour of earlier spectral types for which the indices do not measure TiO. In all fits, stars within the valid range of T_{eff} but deviating more than 3σ from the fitted relation were also rejected.

Finally, for a subsample of stars in common with the stellar library from DTT, we have compared the MgI (DTT) values given in DTT [$\mathrm{MgI\ (DTT)_{DTT}}$] with the ones measured over our spectra. Note that since the measured index is the same in both cases systematic differences between the two sets of measurements could only arise from differences in their spectrophotometric systems. However, no significant differences have been found (Fig. 6c).

To conclude, it is important to remind the reader that the first two calibrations in Table 2 should only be applied once the spectra are on the same spectrophotometric system (i.e. equally flux calibrated and at the same spectral resolution) as the stellar library of CEN01a. If that is not the case, a prior calibration like the last one in Table 2 should be applied before.

2.4 Sensitivities of the new indices to different effects

This section is devoted to characterizing the sensitivity of the indices MgI and sTiO to the S/N, the velocity dispersion broadening (or spectral resolution), relative flux calibration, extinction effects and sky subtraction residuals.

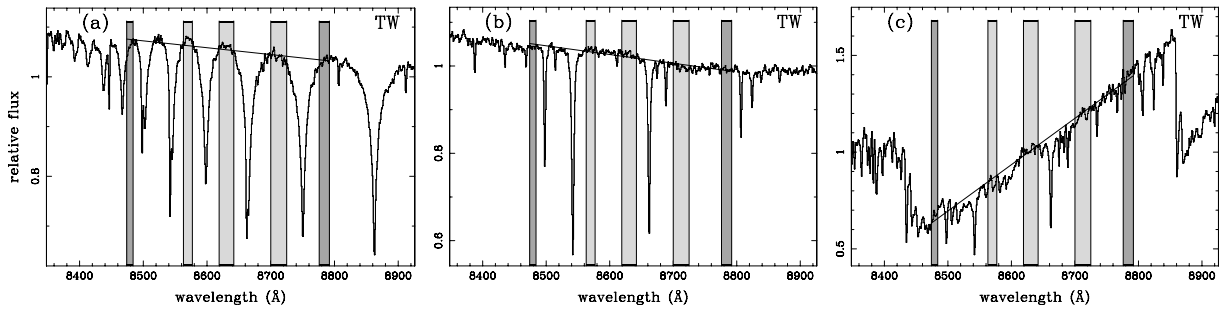

Figure 5. New index definition (this work; TW) for the TiO bands, sTiO, over the same spectral types of Fig. 2. The five continuum bandpasses are those corresponding to the CaT indices in CEN01a. The two bandpasses that define the sTiO value (see equation 1) are illustrated in dark grey.

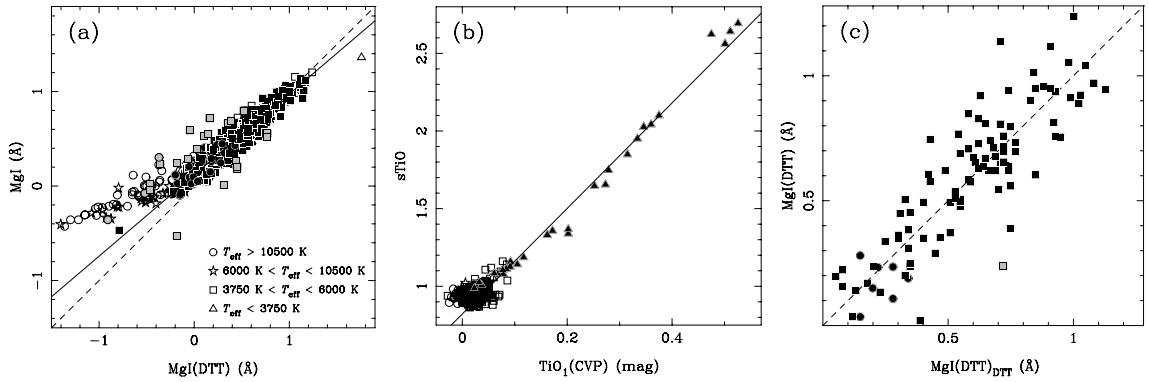

Figure 6. Comparison between the different systems of indices. Diagrams (a) and (b) compare the new indices MgI and sTiO with the corresponding MgI (by DTT) and TiO_1 (by CVP), both measured in this work over the 706 stars of our stellar library (CEN01a). Diagram (c) shows the MgI by DTT measured in our and their spectra [MgI (DTT) and MgI $(DTT)_{DTT}$, respectively] for the subsample of stars in common. Symbol types, indicating different ranges of effective temperature, are given in panel (a). The dashed line in panels (a) and (c) shows the one-to-one relation. Grey symbols are stars deviating more than 3σ from the fitted relation, whereas open symbols refer to those stars with effective temperatures outside the fitted range. The solid line marks the most significant fit to the symbols in black (see Table 2).

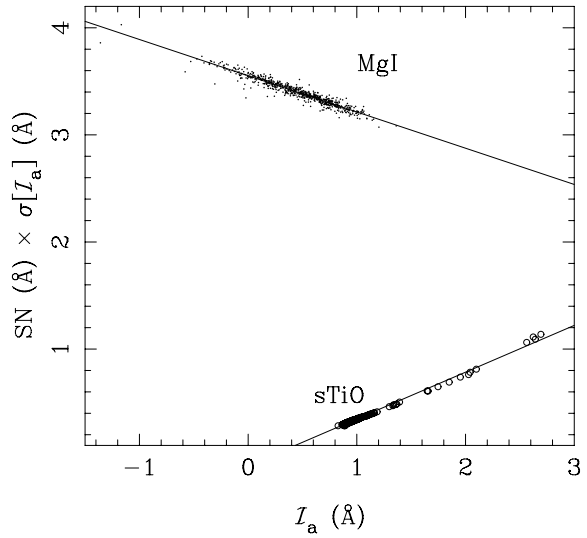

Figure 7. Empirical estimation of the constant factors c_1 and c_2 in equations (3) and (4) for MgI and sTiO, respectively. The least-squares fit to straight lines has been performed rejecting data iteratively outside the 99.73 per cent confidence level.

2.4.1 Signal-to-noise ratio

In CEN01a, a thorough study is presented on the computation of random errors – arising from photon noise – for generic indices. We refer the reader to appendix A2 of that paper for full details about the procedure (see also Cardiel et al. 1998). In those papers, it was demonstrated that it is possible to estimate the predicted random errors of atomic indices as a function of the S/N per angstrom – hereafter SN(Å) – by means of analytical expressions of the form

$$\sigma[\mathcal{I}_a] \simeq \frac{c_1 - c_2\,\mathcal{I}_a}{\mathrm{SN(Å)}}, \qquad (2)$$

where $[\mathcal{I}_a]$ refers to any atomic index (either classical or generic), and the coefficients c_1 and c_2 – which depend on the index definition – can be computed analytically for classical indices, and empirically for generic ones (see appendix 3 in CEN01a).

Following the empirical approach for our generic indices, Fig. 7 displays the product SN(Å) $\times\, \sigma[\mathcal{I}_a]$ versus the index value for all the library stars in CEN01a. As expected for generic atomic indices, MgI exhibits a clear linear relationship, thus supporting previous results that equation (2) is indeed a good approach to the S/N dependence of random errors. Interestingly, although sTiO is not an atomic index, it is also found to follow a nice linear behaviour when included in Fig. 7, despite the fact that it exhibits an opposite trend [what is understandable as slope indices are conceptually different to atomic indices (see Section 2.2.2). Note also that sTiO has no units, so the labels of the axes are not strictly correct in this case]. A least-squares fit to all data provides

$$\sigma[\mathrm{MgI}] \simeq \frac{3.552 - 0.3384\ \mathrm{MgI}}{\mathrm{SN(Å)}}, \qquad (3)$$

and

$$\sigma[\mathrm{sTiO}] \simeq \frac{-0.08914 + 0.4366\ \mathrm{sTiO}}{\mathrm{SN(Å)}}. \qquad (4)$$

As expected, for MgI, c_1 is one order of magnitude larger than c_2, thus reinforcing the idea that photon noise errors in generic atomic indices are barely dependent on the index values. However, this is not the case for slope indices like sTiO. In fact, c_2 dominates the error dependence, in the sense that the larger the index, the larger the error.

Based on the above equations, we estimate that for the typical indices of an old, solar–metallicity SSP (VAZ03) SN(Å) ~ 50 Å^{-1} and ~ 3 Å^{-1} is required to measure, respectively, MgI and sTiO with a 10 per cent uncertainty. It is therefore clear that while sTiO is optimized to be measured on low S/N spectra (a potential application for high-redshift galaxies and extragalactic globular clusters is immediately derived), MgI demands relatively high quality spectra to drive reliable results. This is unavoidably the price one has to pay for defining MgI as a 'pure' Mg indicator, with a very narrow central bandpass that prevents contamination with other nearby lines.

2.4.2 Spectral resolution

With the aim of studying the sensitivity of MgI and sTiO to the spectral resolution or galaxy velocity dispersion broadening (σ), we broadened the whole set of SSP model spectra of VAZ03 by convolving with Gaussians of σ varying from 25 to 400 km s^{-1}, in steps of 25 km s^{-1}. The indices were thus measured for the full set of broadened spectra and, for each model, we fitted a third-order

Table 3. Coefficients of the broadening correction polynomials $\Delta\mathcal{I}/\mathcal{I} = a + b\sigma + c\sigma^2 + d\sigma^3$ for MgI and sTiO, for a representative set of Vazdekis et al. (2003) SSP models of different IMF slopes μ, metallicities [M/H] and ages. $\Delta\mathcal{I}/\mathcal{I}$ is zero for $\sigma = 22.2\,\mathrm{km\,s^{-1}}$, the spectral resolution of the stellar library in CEN01a.

$\mathcal{I}$	μ	[M/H]	Age (Gyr)	$a(\times10^{-3})$	$b(\times10^{-5})$	$c(\times10^{-7})$	$d(\times10^{-9})$
sTiO	1.3	0.0	1.0	0.909	−4.782	3.179	−0.334
	1.3	0.0	12.6	1.421	−7.219	3.764	−0.368
	1.3	−0.7	12.6	0.895	−4.648	2.828	−0.262
	2.8	0.0	1.0	0.753	−3.941	2.536	−0.241
	2.8	0.0	12.6	1.064	−5.434	2.947	−0.296
	2.8	−0.7	12.6	1.145	−5.879	3.333	−0.341
MgI	1.3	0.0	1.0	1030.686	−5544.545	4297.828	−1061.284
	1.3	0.0	12.6	61.862	−207.795	−259.635	−4.898
	1.3	−0.7	12.6	44.553	−124.534	−349.063	27.095
	2.8	0.0	1.0	225.317	−1124.182	539.861	−215.236
	2.8	0.0	12.6	42.790	−127.770	−295.117	10.880
	2.8	−0.7	12.6	37.606	−95.207	−340.763	29.619

polynomial to the relative changes of the index values as a function of velocity dispersion,

$$\frac{\mathcal{I}(\sigma) - \mathcal{I}(\sigma_0)}{\mathcal{I}(\sigma)} = a + b\sigma + c\sigma^2 + d\sigma^3 \equiv p(\sigma), \quad (5)$$

where $\sigma_0 = 22.2\,\mathrm{km\,s^{-1}}$ is the nominal resolution of the VAZ03 models (FWHM = 1.50 Å), and σ is any generic resolution in the same units. Note that equation (5) is computed as a function of the overall spectral resolution, so that for $\sigma = \sigma_0$, $p(\sigma_0) = 0$.

Table 3 provides the derived coefficients for MgI and sTiO measured over a number of representative SSP models. Fig. 8 illustrates the obtained ΔMgI/MgI and ΔsTiO/sTiO values for this set of representative models. The grey region represents the locus of broadening corrections for the whole SSP model spectral library.

It is worth noting that, thanks to the high stability of the continuum bandpasses, the index sTiO is formally insensitive to broadening, with largest corrections being only ∼1 per cent at $\sigma \sim 400\,\mathrm{km\,s^{-1}}$. On the other hand, MgI turns out to be quite dependent on spectral resolution. This is due to the small width of the central bandpass – chosen this way to preserve as much as possible the Mg abundance sensitivity – and to the intrinsic weakness of the Mg I line (EW < 1 Å). In fact, at $\sigma = 300\,\mathrm{km\,s^{-1}}$, MgI decreases by ∼78.2 ± 6.6 per cent w.r.t. the value at $\sigma_0 = 22.2\,\mathrm{km\,s^{-1}}$, with uncertainties accounting for the different broadenings derived from the full set of SSPs. This effect decreases down to ∼56.8 ± 0.6 per cent at $\sigma = 200\,\mathrm{km\,s^{-1}}$, which can be considered as a reasonable limiting resolution to neglect broadening correction differences due to distinct SSP templates.

As already discussed in VAZ03 for the Ca II triplet indices, the use of SSP model spectra to match the effects of galaxy broadening is a better approach than the use of single stellar spectra, as the latter shows even large variations among different spectral types. In any case, the user should still keep in mind that systematic differences – arising, for instance, from different abundance ratios or local flux calibration mismatches – may exist between real galaxies and the best-matched SSP models. For this reason, whenever feasible, an alternative approach is that of broadening the galaxy spectra and the SSP models up to the largest spectral resolution of the galaxy sample. The success of this approach for the MgI and sTiO indices of elliptical galaxies over a range in mass was illustrated in Cenarro et al. (2003).

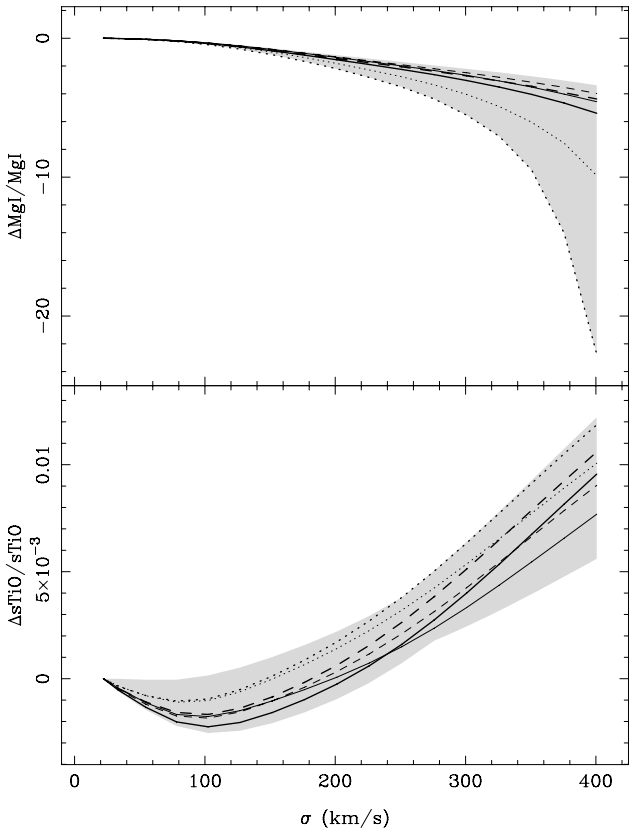

Figure 8. Broadening correction ΔMgI/MgI and ΔsTiO/sTiO as a function of total σ. Corrections have been computed by convolving model spectra by VAZ03 with Gaussians from $\sigma = 25$ to $400\,\mathrm{km\,s^{-1}}$ in steps of $25\,\mathrm{km\,s^{-1}}$. $\Delta I/I$ is zero for $\sigma = 22.2\,\mathrm{km\,s^{-1}}$ (the spectral resolution of the stellar library in CEN01a). Different line types are employed to illustrate the broadening corrections for a set of representative models of different ages, metallicities and IMFs: solid (12.6 Gyr, [M/H] = 0.0), dotted (1.0 Gyr, [M/H] = 0.0) and dashed (12.6 Gyr, [M/H] = −0.7), with thick and thin lines corresponding to IMF slopes of $\mu = 1.3$ (Salpeter) and 2.8, respectively. The polynomial coefficients of such broadening corrections are given in Table 3. The grey area illustrates the region covered by the broadening corrections obtained for the whole set of SSP spectra of VAZ03.

2.4.3 *Flux calibration and reddening correction*

There is not a simple recipe to analytically quantify the sensitivity of an index to the uncertainties in the relative flux calibration, as it does depend not only on the index definition itself, but also on the uncertainties of the response curves derived for a given observing run. In general, the sensitivity of any spectroscopic index to flux calibration gets larger as the spectral coverage of its sidebands increases. In this sense, it is clear that sTiO is particularly sensitive to systematics in the flux calibration and the reddening correction, as it basically measures the slope of the pseudo-continuum in a spectral window of ∼300 Å. For instance, assuming the Galactic interstellar extinction of Fitzpatrick (1999), the effect of reddening in the sTiO index is given by

$$\frac{\mathrm{sTiO_{ext}} - \mathrm{sTiO_0}}{\mathrm{sTiO_0}} = 0.087 \times E(B-V), \quad (6)$$

where $\mathrm{sTiO_{ext}}$ is the reddened index value [for a colour excess of $E(B-V)$ and $R = 3.1$] and $\mathrm{sTiO_0}$ the extinction corrected one. This means that to ensure systematics in the sTiO index below 1 per cent, reddening correction uncertainties should not be larger

than $E(B-V) \sim 0.1$ mag. MgI, however, is basically stable under flux calibration variations and extinction corrections.

As will be discussed in Section 3.3.2 with the aim of explaining the observed FF residuals, it is important to note that the main source of random errors for the sTiO index turns out to be the random uncertainties in the determination of the response curve. This stresses the importance of an accurate flux calibration and extinction correction before performing any meaningful comparison between evolutionary synthesis model predictions and measured spectra.

2.4.4 Sky emission lines and telluric absorptions

Sky emission lines – produced by the OH radical (e.g. Rousselot et al. 2000) – and telluric absorptions – due to water vapour and other molecules (e.g. Stevenson 1994; Chmielewski 2000) – are common features at the near-IR spectral range. A careful data reduction is necessary for a proper removal of these effects, although a detailed description of specific techniques is out of the scope of this paper. Rather than that, we just aim to compare, qualitatively, the potential sensitivities of our indices to the above contaminations. An absolute study is not possible at this point, as it would strongly depend on the quality of the final spectra.

Because of the narrow index definition and the intrinsic weakness of the Mg I line, MgI is quite more sensitive to sky line and telluric absorption residuals than sTiO. In principle, since the sTiO slope is well constrained by five continuum bandpasses, a few deviating pixels in its continuum bandpasses would not alter the index value significantly (actually, generic indices are particularly insensitive to sky line residuals; Section 2.2). A different situation would be that in which a strong – not properly removed – telluric absorption is affecting the red – or blue – sides of the index definition. In this case, the local slope of the continuum would be fictitiously biased and the index would be highly unreliable. Fortunately, this is not the case for spectra at the local rest frame (like the stellar library of CEN01a). In any case, it is worth noting that the strong telluric absorption at $\lambda \gtrsim 8940$ Å may affect the MgI and sTiO indices of objects with radial velocities larger than ∼3200 and 5000 km s^{-1}, respectively.

3 THE DEPENDENCE OF THE MgI LINE AND TiO BANDS ON THE STELLAR ATMOSPHERIC PARAMETERS

3.1 Qualitative behaviour

As a first step to understand the behaviour of the Mg I line and TiO bands as a function of the stellar atmospheric parameters, this section describes, from a qualitative point of view, the effects of effective temperature ($T_{\rm eff}$ or $\theta \equiv 5040/T_{\rm eff}$), surface gravity ($\log g$) and metallicity ([Fe/H]) on the strength of both spectral features. Fig. 9 illustrates the MgI and sTiO indices versus θ for all the stars in CEN01a.

3.1.1 The stellar atmospheric parameters

The stellar atmospheric parameters employed throughout this work are those derived in CEN01b, where, after an exhaustive compilation from several hundreds of bibliographic sources, the different sources were calibrated and corrected on to the system established by Soubiran, Katz & Cayrel (1998) to end up with a homogeneous

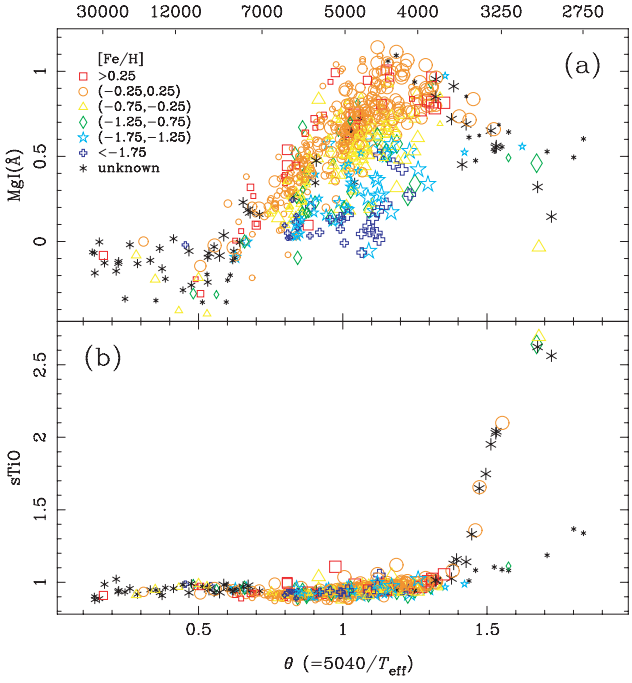

Figure 9. MgI and sTiO indices versus θ ($\equiv 5040/T_{\rm eff}$) for the whole stellar library in CEN01a. Different symbols are used to indicate different ranges of metallicities (as in the key), while sizes are related with surface gravity, in the sense that the smaller the symbol (dwarfs), the higher the gravity. On the top, the effective temperature scale is given.

set of atmospheric parameters (see details in CEN01b). Although more recent determinations of $T_{\rm eff}$, $\log g$ and/or [Fe/H] have appeared since 2001 for some library stars, we preferred to keep the parameters quoted in CEN01b to preserve full consistency with the CaT, PaT and CaT* FFs given in CEN02, as well as with the corresponding SSP SEDs predicted in VAZ03. It is worth noting that, in Cenarro et al. (2007), an updated extension of the compiling work in CEN01b was carried out for MILES, which in turn includes 403 stars in common with CEN01a. Using all those stars in CEN01a for which any of the three atmospheric parameters in Cenarro et al. (2007) was updated with respect to CEN01b (194 stars in $T_{\rm eff}$, 133 in $\log g$ and 116 in [Fe/H]), we determined that the differences between the old and new final determinations are null on average, with rms standard deviations of $\sigma\ T_{\rm eff} \sim 72$ K, $\sigma\ \log g \sim 0.22$ dex and σ[Fe/H] ~ 0.1 dex. Since there exist not statistically significant offsets between both data sets in any of the three atmospheric parameters that may lead to systematic effects, and the scatter of the distributions is smaller than the typical uncertainties in the atmospheric parameters (see Section 3.3.1), we are confident that using the parameters in CEN01b is not at all a compromise on the quality of the results that we present in this work.

3.1.2 The Mg I line

As it is expected for any metal line, Mg I shows a negligible strength in the spectra of the earliest spectral types (see the upper spectrum in Fig. 1) which are mainly dominated by strong absorption Paschen lines. Therefore, high-temperature stars have null MgI values, or even below zero (Fig. 9a). The latter occurs since, in this kind of stars, the index pseudo-continuum lies slightly below the true level, thus leading to negative values when the Mg I line is very weak. For latter spectral types, the Mg I strength increases with the decreasing

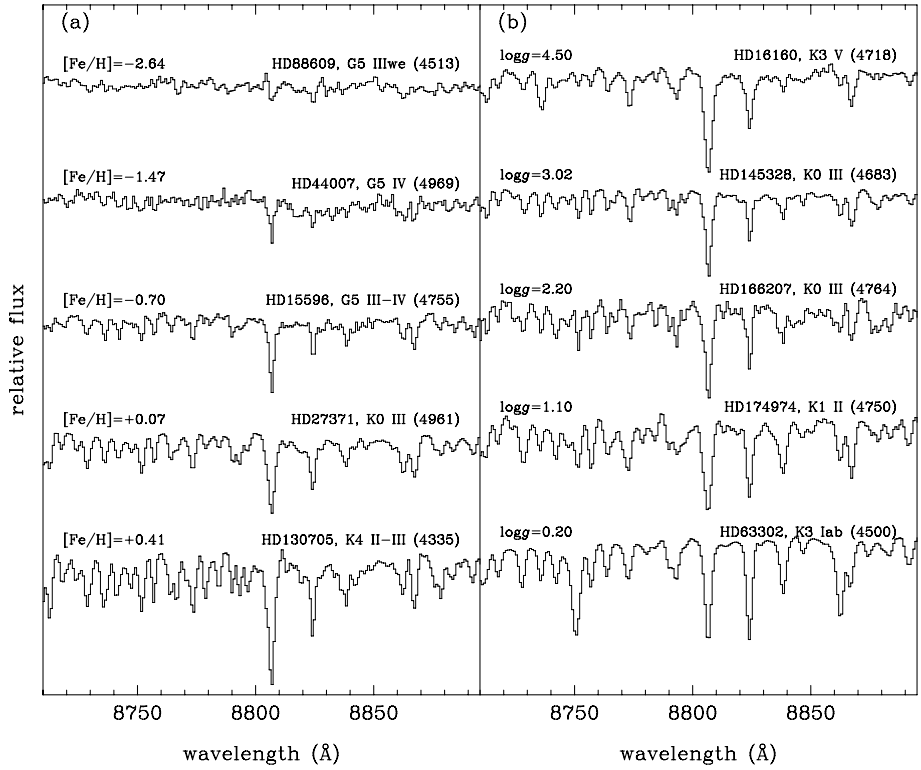

Figure 10. Metallicity and gravity effects on the strength of the Mg I line at 8807 Å for a subsample of stars from CEN01a. Panel (a) shows stars with similar temperature and gravity but spanning a wide range in metallicity. Panel (b) displays a sequence in gravity for stars with similar temperature and metallicity around solar. Temperatures in kelvin are given in brackets. All the spectra have been normalized and reproduced using the same scale. It is clear that the Mg I line strength increases with [Fe/H]. The effect of log g on the strength of the Mg I line is very mild, with intermediate log g stars having slightly weaker lines.

temperature. This behaviour peaks at $T_{\rm eff} \sim 4000$–5000 K before decreasing for mid- and late-M types. For a wide range of spectral types ($3500 \lesssim T_{\rm eff} \lesssim 7000$ K), the Mg I line is also heavily affected by metallicity and gravity effects, leading to the spread of MgI values in Fig. 9(a).

The effects of metallicity and gravity on the Mg I line are also illustrated in Fig. 10, where two comparative sequences in (a) metallicity and (b) surface gravity for several G–K spectral types from CEN01a around the Mg I line are shown. From Figs 9(a) and 10(a), it is clear that MgI increases as metallicity increases. On the contrary, the weak, subtle dependence on gravity is difficult to distinguish at first sight. Only when a detailed, statistical analysis is carried out, it is possible to detect that dwarfs and supergiant stars exhibit slightly larger MgI indices than normal giants. The empirical FFs derived in the next section will account for such behaviour.

3.1.3 The TiO bands

As already mentioned in Section 2, molecular bands of TiO and VO appear in the spectra of early M-types, increasing their strength with the decreasing temperature. Fig. 11 shows a comparative sequence in late M-types for a sample of dwarfs (a) and giants (b) from CEN01a. For a given temperature, giant stars exhibit molecular bands quite stronger than those in dwarf stars. Also, the strengthening rate of these bands with the decreasing temperature is larger in giant stars. The last behaviours are apparent in Fig. 9(b), suggesting that such TiO bands can certainly be used as a powerful dwarf-to-giant discriminator for cold spectral types (see e.g. Gilbert et al. 2006). For $T_{\rm eff} \lesssim 3600$ K ($\theta \gtrsim 1.4\,{\rm K}^{-1}$), the index sTiO of dwarfs and giants clearly follows two different, increasing trends. The rest of spectral types exhibit sTiO $\lesssim 1$. It makes sense since the local continuum of their spectra is roughly flat. In spite of that, for this regime of temperatures there exists a weak gravity dependence in the sense that the lower the gravity the larger the index. It just arises from the fact that the shape of the continuum slightly varies with the luminosity class.

3.2 The fitting functions

In this section, we present the empirical calibration of the new indices in terms of the stellar atmospheric parameters. The outputs of this procedure are the so-called FFs, polynomials that can be easily implemented into SSP codes to predict the integrated indices of a wide variety of stellar systems (e.g. Gorgas et al. 1993; Worthey et al. 1994; Worthey & Ottaviani 1997; Gorgas et al. 1999; CEN02; Schiavon 2007; Mármol-Queraltó et al. 2008; Maraston et al. 2009).

The general procedure followed to compute the FFs is the same as in CEN02, so we refer the reader to that paper for a detailed description of the method. These FFs have been calculated using the index measurements presented in Section 2.2.3 and the atmospheric parameters derived in CEN01b. It is important to remind that the FFs are only mathematical representations of the behaviour of the indices as a function of the atmospheric parameters and, thus, a physical justification of the derived coefficients is beyond the scope of this paper.

Readers interested in employing these FFs can use the FORTRAN routine available at http://www.ucm.es/info/Astrof/ellipt/MgIsTiO.html. This program performs the required

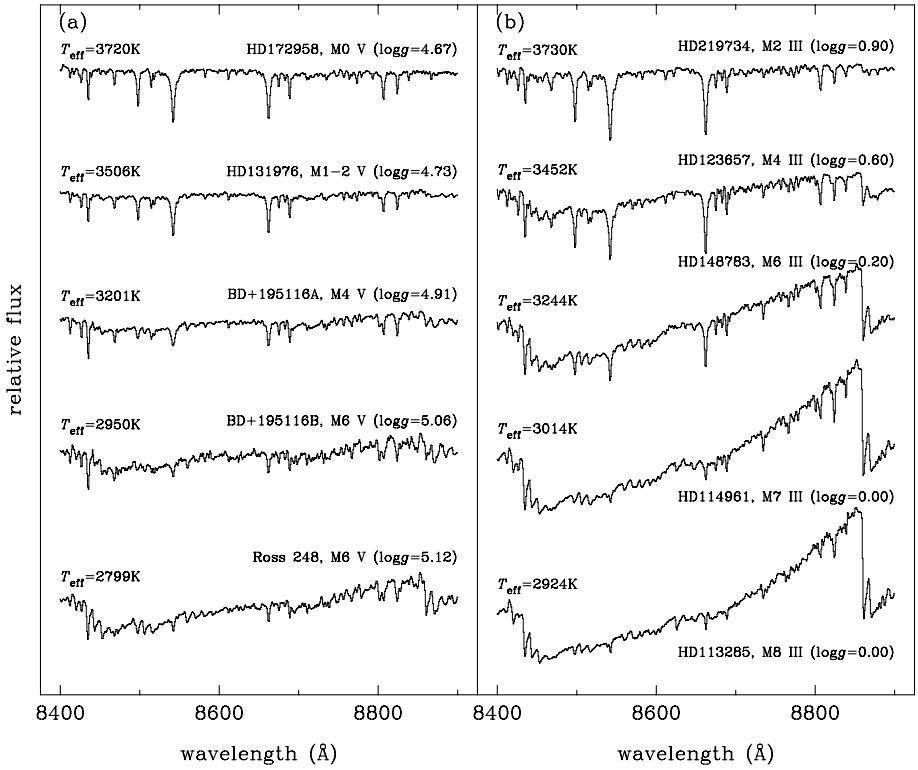

Figure 11. Sequences in M-types for (a) dwarf and (b) giant stars from CEN01a. Effective temperatures, names, spectral types, luminosity classes and surface gravities ($\log g$ in dex) are given in the labels. All the spectra have been normalized and reproduced using the same scales, so relative differences among the spectra are kept. At a fixed temperature, TiO bands in giants are stronger than in dwarfs. For both luminosity classes, the strength of the TiO bands increases with the decreasing temperature.

interpolations to provide the MgI and sTiO indices (together with CaT*, CaT and PaT) as a function of the three input atmospheric parameters. It also gives an estimation of the errors in the index predictions, as explained in Section 3.3.

3.2.1 The fitting procedure

Following the same procedure as that in CEN02, we use θ, $\log g$ and [Fe/H] as effective temperature, surface gravity and metallicity indicators. The FFs have been computed as polynomials of the atmospheric parameters with terms up to the third order, including all possible cross-terms among the parameters. Two possible functional forms are computed,

$$\mathcal{I}_{\rm a}(\theta, \log g, [{\rm Fe/H}]) = p(\theta, \log g, [{\rm Fe/H}]) \quad \text{or} \tag{7}$$

$$\mathcal{I}_{\rm a}(\theta, \log g, [{\rm Fe/H}]) = \text{const.} + \exp\left[p(\theta, \log g, [{\rm Fe/H}])\right], \tag{8}$$

keeping the one that minimizes the residuals of the fit. $\mathcal{I}_{\rm a}$ refers to any of the above indices and p is a polynomial

$$p(\theta, \log g, [{\rm Fe/H}]) = \sum_{0\le i+j+k\le 3} c_{i,j,k}\theta^i(\log g)^j[{\rm Fe/H}]^k, \tag{9}$$

with $0 \le i + j + k \le 3$ and $0 \le i, j, k$.

Given the wide parameter space covered by the stellar sample and the complex behaviour of the indices MgI and sTiO, we proceeded as in CEN02 and divided the whole parameter space into several boxes of parameters in which local FFs can be properly computed. A final FF for the whole parameter space has been constructed by interpolating the derived local functions. In order to do that, the boundaries of the boxes were defined in such a way that they overlapped, including thus several stars in common. In the overlapping zones, cosine-weighted means of the functions corresponding to both boxes were performed to guarantee a smooth interpolation (see CEN02).

The local FFs were derived through a weighted least-squares fit to all the stars within each parameter box, with weights according to the uncertainties of the indices for each individual star, as given in Section 2.2.3. Since not all the 20 possible terms were necessary, we followed a systematic procedure to obtain the appropriate local FF in each case. It made use of statistical criteria to accept or reject each single term depending on its significance level (see CEN02 for further details). Finally, the final combination of terms was the one which provided the minimum unbiased residual variance.

During the fitting procedure for the MgI and sTiO indices, 21 and 16 stars were, respectively, rejected as they were found to exhibit large residuals w.r.t. the final fits, or were subject to have anomalous behaviours. Such stars are indicated in Table 4. Many of them are variable, binary, or emission line stars, whilst some other stars just have unreliable features affecting the index measurement because of very low S/N, cosmetic defects, etc. For identical reasons, most of them were already rejected for the final CaT*, CaT and PaT FFs in CEN02.

The derived local FFs for the indices MgI and sTiO are presented, respectively, in Tables 5 and 6. The tables are subdivided according to the atmospheric parameter ranges of each fitting box and include the functional forms of the fits (polynomial or exponential), the significant coefficients and their corresponding formal errors, the typical index error for the N stars employed in each interval ($\sigma^2_{\rm typ} = N/\sum_{i=1}^{N}\sigma_i^{-2}$), the unbiased residual variance of the fit ($\sigma^2_{\rm std}$) and

Table 4. List of stars which were rejected during the FF computation. The diagnostics for rejection are coded as: C, carbon star; EmL, emission lines of the elements in brackets; P, pulsating star; SB, spectroscopic binary; Var, variable star; *: bad-quality spectrum because of low S/N, bad exposing conditions, unreliable spectral features and others.

Name	Diagnostic	Name	Diagnostic
HD 108	EmL (Ca, H)	HD 112014	SB
HD 1326B	Flare star	HD 120933	Var (CVn)
HD 17491	P	HD 121447	Var
HD 35601	P	HD 181615	EmL (Ca)
HD 37160	* MgI	HD 217476	Var
HD 39801	* MgI	BD+ 61 154	EmL (Ca,H)
HD 42475	P	NGC 188 II-72	* MgI
HD 46687	C	M92 I-10	* MgI
HD 54300	C	M92 I-13	* MgI & sTiO
HD 58972	SB	M92 II-23	* MgI & sTiO
HD 74000	* MgI		

the determination coefficient (r^2). Note that this coefficient provides the fraction of the index variation in the sample which is explained by the derived FFs.

3.2.2 *MgI fitting functions*

At both ends of the temperature regime covered by our stellar library, MgI exhibits a different behaviour for dwarf stars, on one side, and giant and supergiants stars, on the other. This is why we defined separate boxes in Table 5 to compute the corresponding local fits: *a* and *b* for hot dwarfs and giants, and *e* and *f* for cold dwarfs and giants. No terms in $\log g$ and [Fe/H] were found to be statistically significant in any of the two luminosity bins, so only terms in θ were needed. However, for intermediate temperatures (warm and cool stars; boxes *c* and *d* in Table 5), the three atmospheric parameters play an important role in reproducing the complex behaviour of the MgI index.

Figs 12(a), (b) and (c) illustrate the general FFs (i.e. the interpolation of all the local FFs) for three gravity bins that typically represent supergiants, giants and dwarfs, respectively. As expected, there exists a clear dependence on metallicity and θ at intermediate temperatures in the sense that MgI increases with the increasing [Fe/H] and the decreasing temperature. Fig. 12(d) displays the derived FFs for solar metallicity and different gravity values. Apart from reinforcing the strong temperature dependence of the MgI index, this figure illustrates that gravity effects are not negligible at intermediate temperatures. As a matter of fact, there exists a sort of degeneracy in the sense that dwarf stars (thinnest solid lines; $\log g \sim 4$–5) and supergiant stars (thickest solid lines; $\log g \sim 0$–1) reach similar MgI values, which are systematically larger than those of giants with intermediate $\log g$ values.

It is important to note that, while the lines in Fig. 12 correspond to projections of the FFs at particular values of $\log g$ and [Fe/H], the plotted stars span a range of atmospheric parameters around these central values. Therefore, it is not expected that the lines fit exactly all the points in the plots. In any case, there are still some curves which do not appear to be well constrained by the observations in certain regions of the parameter space. For instance, there are no stars for $\theta < 0.5$ in Fig. 12(a) ($\log g = 1.0$) and for $\theta > 1.3$ in Fig. 12(b) ($\log g = 2.6$). Stars with these parameters just do not exist, and therefore they will never be required by the stellar population models.

Table 5. Coefficients and statistical data of the local FFs for the index MgI in each range of atmospheric parameters. The term 'giant' also includes supergiant stars.

(a) Hot dwarfs		$0.13 < \theta < 0.70$	$2.80 < \log g < 4.50$
Exponential fit		Const. $= -1.50$	$N = 49$
c_0	:	0.4284 ± 0.0936	$\sigma_{\rm typ} = 0.046$
θ^2	:	-4.833 ± 1.137	$\sigma_{\rm std} = 0.094$
θ^3	:	7.476 ± 1.485	$r^2 = 0.74$
(b) Hot giants		$0.13 < \theta < 0.60$	$1.20 < \log g < 3.01$
Polynomial fit			$N = 21$
c_0	:	-0.1202 ± 0.0371	$\sigma_{\rm typ} = 0.033$
θ^3	:	0.6254 ± 0.2572	$\sigma_{\rm std} = 0.056$
			$r^2 = 0.47$
(c) Warm stars		$0.30 < \theta < 1.30$	$0.00 < \log g < 5.00$
Polynomial fit			$N = 586$
c_0	:	1.846 ± 0.423	$\sigma_{\rm typ} = 0.044$
θ	:	-7.960 ± 1.650	$\sigma_{\rm std} = 0.094$
$\log g$	:	-0.1999 ± 0.0349	$r^2 = 0.89$
θ [Fe/H]	:	0.3079 ± 0.0310	
θ^2	:	11.68 ± 2.02	
[Fe/H]^2	:	0.1862 ± 0.0600	
$\theta^2 \log g$	:	-0.06817 ± 0.03318	
θ^3	:	-4.571 ± 0.760	
θ [Fe/H]^2	:	-0.1624 ± 0.0605	
$\theta \log^2 g$	:	0.05072 ± 0.00568	
(d) Cool stars		$1.05 < \theta < 1.35$	$0.00 < \log g < 5.00$
Polynomial fit			$N = 230$
c_0	:	-9.005 ± 3.563	$\sigma_{\rm typ} = 0.039$
θ	:	16.76 ± 6.00	$\sigma_{\rm std} = 0.099$
θ [Fe/H]	:	1.711 ± 0.641	$r^2 = 0.76$
$\theta \log g$	:	-0.1262 ± 0.0400	
θ^2	:	-6.941 ± 2.516	
[Fe/H]^2	:	0.8445 ± 0.4527	
$\log^3 g$	:	0.007011 ± 0.001746	
θ^2 [Fe/H]	:	-1.247 ± 0.536	
θ [Fe/H]^2	:	-0.7490 ± 0.3924	
(e) Cold dwarfs		$1.07 < \theta < 1.90$	$4.40 < \log g < 5.20$
Polynomial fit			$N = 22$
c_0	:	2.638 ± 0.469	$\sigma_{\rm typ} = 0.039$
θ^2	:	-2.098 ± 0.678	$\sigma_{\rm std} = 0.085$
θ^3	:	0.805 ± 0.306	$r^2 = 0.90$
(f) Cold giants		$1.30 < \theta < 1.80$	$0.00 < \log g < 1.65$
Polynomial fit			$N = 27$
c_0	:	1.896 ± 0.254	$\sigma_{\rm typ} = 0.023$
θ^2	:	-0.5762 ± 0.1161	$\sigma_{\rm std} = 0.157$
			$r^2 = 0.74$

Because of the complicated functional form of MgI at intermediate temperatures as compared to that of cold stars, the local fit in Table 5 (part d) was specially designed to preserve smoothness when interpolating the local fits of warm and cold stars. Even so, a fictitious peak in the FFs of very metal poor ([Fe/H] ~ -2.0) giants and supergiants at $\theta \sim 1.2$ is still apparent in Figs 12(a) and (b). This is in part due to the lack of reliable metallicity determinations for very cold stars, which prevents us from a more accurate calibration of metallicity effects all over the $\theta - \log g$ space. As a matter of fact, there exists a stronger limitation arising from the intrinsic absence of metal-poor, very cold giant stars, as the red giant and asymptotic giant branches of so metal-poor populations – like, e.g., the globular cluster M92 – do not reach so low temperatures. Once again, we are confident that the above interpolation is not having an important

Table 6. Coefficients and statistical data of the local FFs for the index sTiO in each range of atmospheric parameters. The term 'giant' also includes supergiant stars.

(a) Hot dwarfs		$0.13 < \theta < 0.65$	$2.81 < \log g < 4.37$
Exponential fit		const. $= 0.78$	$N = 35$
c_0	:	-2.261 ± 0.059	$\sigma_{\rm typ} = 0.004$
θ^2	:	8.062 ± 0.916	$\sigma_{\rm std} = 0.013$
θ^3	:	-11.07 ± 1.31	$r^2 = 0.78$
(b) Hot giants		$0.13 < \theta < 0.85$	$0.39 < \log g < 3.01$
Polynomial fit			$N = 40$
c_0	:	0.9551 ± 0.0066	$\sigma_{\rm typ} = 0.003$
			$\sigma_{\rm std} = 0.030$
			$r^2 = 0.61$
(c) Warm stars		$0.60 < \theta < 1.30$	$0.00 < \log g < 4.85$
Polynomial fit			$N = 569$
c_0	:	1.855 ± 0.223	$\sigma_{\rm typ} = 0.004$
θ	:	-2.618 ± 0.700	$\sigma_{\rm std} = 0.015$
$\log g$	:	-0.07343 ± 0.01508	$r^2 = 0.75$
[Fe/H]	:	0.03046 ± 0.00511	
θ^2	:	2.691 ± 0.726	
$\log^2 g$	:	0.01767 ± 0.00661	
$\log g$ [Fe/H]	:	-0.008611 ± 0.001667	
θ^3	:	-0.8813 ± 0.2471	
$\log^3 g$	:	-0.001651 ± 0.000857	
(d) Cold dwarfs		$1.07 < \theta < 1.90$	$4.45 < \log g < 5.13$
Polynomial fit			$N = 21$
c_0	:	2.454 ± 0.296	$\sigma_{\rm typ} = 0.004$
θ	:	-2.547 ± 0.418	$\sigma_{\rm std} = 0.017$
θ^2	:	1.070 ± 0.145	$r^2 = 0.98$
(e) Cold giants		$1.28 < \theta < 1.47$	$0.00 < \log g < 2.00$
Polynomial fit			$N = 25$
c_0	:	5.997 ± 1.925	$\sigma_{\rm typ} = 0.003$
θ^2	:	-9.245 ± 3.119	$\sigma_{\rm std} = 0.024$
θ^3	:	4.837 ± 1.524	$r^2 = 0.95$
(f) Very cold giants		$1.40 < \theta < 1.80$	$0.00 < \log g < 1.65$
Polynomial fit			$N = 14$
c_0	:	-39.79 ± 5.45	$\sigma_{\rm typ} = 0.006$
θ	:	37.44 ± 5.24	$\sigma_{\rm std} = 0.006$
θ^3	:	-4.319 ± 0.709	$r^2 = 0.99$

effect on the integrated MgI values computed for low-metallicity SSPs.

It is worth noting here that apart from studying the behaviour of the Mg I line DTT also calibrated the strength of the MgI (DTT) index as a function of the stellar atmospheric parameters. By performing a principal component analysis for the 106 stars of their library (F5 to M1 spectral types), they derived a biparametrical linear dependence on metallicity and effective temperature – with no sensitivity to surface gravity – so that MgI (DTT) increases with the increasing [Fe/H] and the decreasing $T_{\rm eff}$. In spite of the parameter coverage of the DTT stellar sample allowing to detect the weak dependence on $\log g$ and other significant terms, they restricted their analysis to the first two principal components, which explain the simple dependence reported in their work. For this reason, the DTT calibration, although useful for achieving a first-order understanding of the MgI behaviour, should not be considered as an accurate input ingredient for SSP modelling. As a matter of fact, a simple extrapolation of the DTT calibration to larger and lower temperatures fails to reproduce, among other, the observed MgI turnover at $\theta \sim 1.2$ (after which MgI decreases with the decreasing $T_{\rm eff}$) and the MgI plates for the earliest spectral types.

3.2.3 sTiO fitting functions

As described in Section 3.1.3, the index sTiO exhibits values around 1 – or slightly smaller – for most library stars except for the latest spectral types, for which the index increases with the decreasing temperature. Boxes *d*, *e* and *f* in Table 6 were designed to reproduce, separately for dwarf and giant stars, the increasing sTiO trend at the low-temperature regime. Only terms in θ were necessary, as it also happens for the earliest spectral types (boxes *a* and *b*).

In spite of the apparent constancy of the sTiO values for intermediate temperatures, terms in all the three atmospheric parameters turned out to be statistically significant in box *c*, with the [Fe/H] dependence being the less important. For this reason, Fig. 13 – for solar metallicity and different gravities – suffices to illustrate the general FFs of the sTiO index. Apart from the strong sTiO increase with the decreasing temperature (particularly for cold giant stars), the gravity effect at the intermediate-temperature regime is worth noting, in the sense that the larger the gravity (dwarfs; thinnest solid lines), the lower the sTiO index.

3.3 Residuals and error analysis

Defining the index residual of a given star as the difference between the observed index and the one predicted by the FFs ($\Delta\mathcal{I} = \mathcal{I}_{\rm obs} - \mathcal{I}_{\rm pred}$), Figs 14 and 15 show the residuals of the indices MgI and sTiO for the whole stellar library as a function of θ. These residuals are given for each star in Table 10. Overall, no systematic deviations are found for any of the three atmospheric parameters. Star clusters have also been analyzed separately and, except for the MgI values of the open cluster M67, no systematic effects have been found. We defer the analysis of this particular case to Section 3.4, where the effect of different [Mg/Fe] ratios on the MgI FF residuals is discussed.

To explore in more detail the reliability of the present FFs, in Table 7 we list the unbiased residual standard deviation from the fits, $\sigma_{\rm std}$, the typical error in the measured indices arising from photon noise and radial velocity uncertainties, $\sigma_{\rm typ}$, and the determination coefficient, r^2, for all the stars employed in the computation of the general FFs. It is important to note that, apart from the outlier stars rejected from the fits, a few stars with unknown [Fe/H] could not be included in the metallicity-dependent fits and no residuals were therefore computed. It is clear that for both indices $\sigma_{\rm std}$ is larger than expected uniquely from typical errors (see also the partial values of $\sigma_{\rm std}$ and $\sigma_{\rm typ}$ in Tables 5 and 6), which suggests that the FF residuals must be dominated by other effects. In CEN02, it was demonstrated that the errors in the input parameters were the main source of residuals for the FFs of the Ca II indices. We therefore perform a similar analysis to constrain the effect of the atmospheric parameter uncertainties in the residuals of the MgI and sTiO FFs. Aimed at constraining the potential sensitivity of sTiO to small changes in the continuum shape, the effect of flux calibration uncertainties is also discussed.

3.3.1 Uncertainties in the stellar atmospheric parameters

We have computed how the errors in the input atmospheric parameter of the library stars translate into uncertainties in the predicted indices. Since this depends on both the local functional form of the

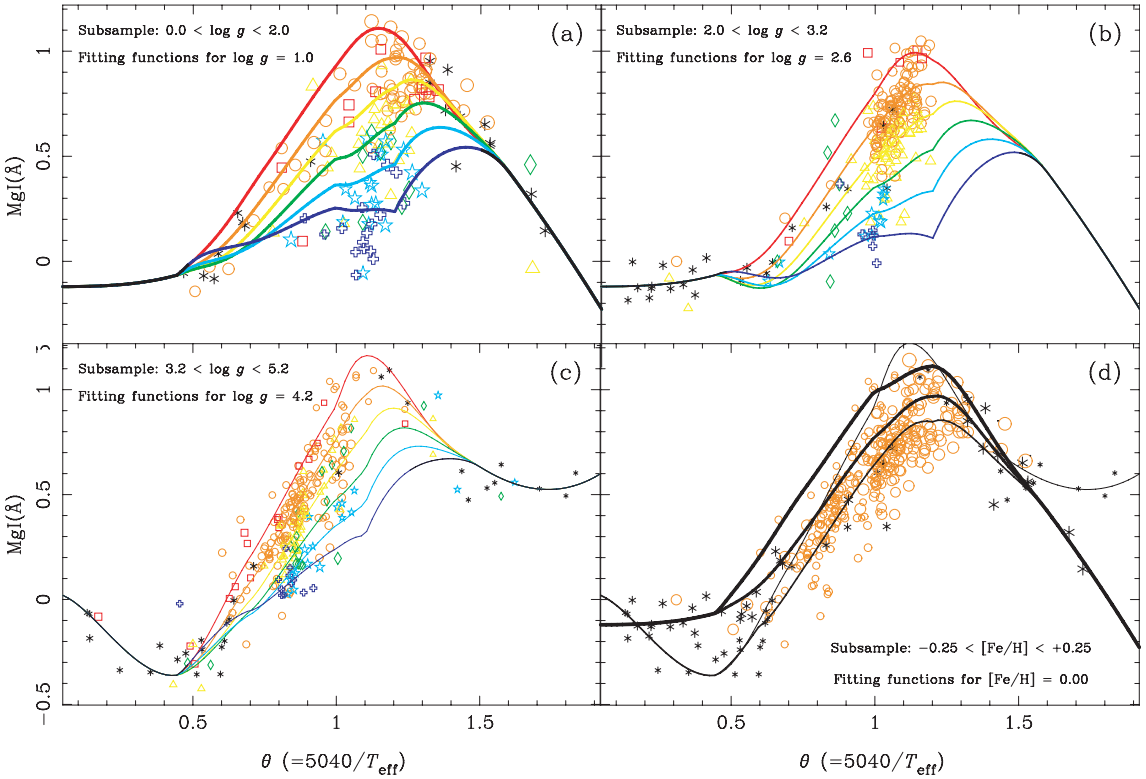

Figure 12. MgI values and general FFs for different atmospheric parameter regimes. Panels (a), (b) and (c) display, respectively, all the stars with gravities in the ranges $0.0 \leq \log g < 2.0$, $2.0 \leq \log g < 3.2$ and $3.2 \leq \log g < 5.2$, together with the derived FFs for the mean gravity in each range, i.e. $\log g = 1.0$ (a), 2.6 (b) and 4.2 (c). In the mid-temperature range, the different lines represent, from top to bottom, the functions for metallicities [Fe/H] = +0.5, 0.0, −0.5, −1.0, −1.5 and −2.0, whilst, for high and low temperatures, the FFs do not depend on metallicity. Panel (d) shows all the stars around solar metallicity ($-0.25 <$ [Fe/H] $\leq +0.25$) and the corresponding FFs computed for [Fe/H] = 0.0 and different values of gravity ($\log g$ = 0.0, 1.0, 3.0 and 5.0, from the thickest to the thinnest line). Codes and relative sizes of the star symbols (indicating, respectively, metallicity and gravity ranges) are explained in Fig. 9(a). Note that while the lines displayed here correspond to FFs at particular values of $\log g$ and [Fe/H], the plotted stars span a range of atmospheric parameters around these central values. This is the reason why the lines do not exactly fit all the points in the plots. Also note that these FFs have not been derived by using only these plotted stars, but also the whole sample.

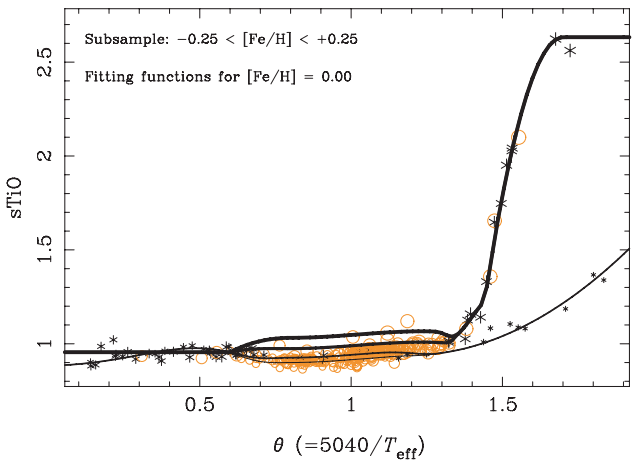

Figure 13. sTiO values for all the stars around solar metallicity ($-0.25 <$ [Fe/H] $\leq +0.25$). The curves correspond to general FFs computed for [Fe/H] = 0.0 and different values of gravity ($\log g$ = 0.0, 1.0, 3.0 and 5.0, from the thickest to the thinnest line). Codes and relative sizes of the star symbols (indicating, respectively, metallicity and gravity ranges) are explained in Fig. 9(a).

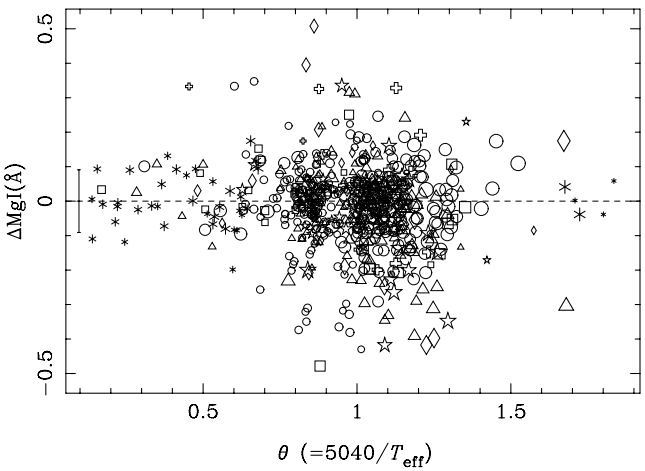

Figure 14. Residuals of the MgI FFs ($\Delta\mathrm{MgI} = \mathrm{MgI_{obs}} - \mathrm{MgI_{pred}}$) versus θ for the whole stellar library [see Fig. 9(a) for symbol codes]. The error bar at the left-hand margin indicates the unbiased residual standard deviation of the fit. See text in Sections 3.3 and 3.4 for a study on the different error sources driving the observed residuals.

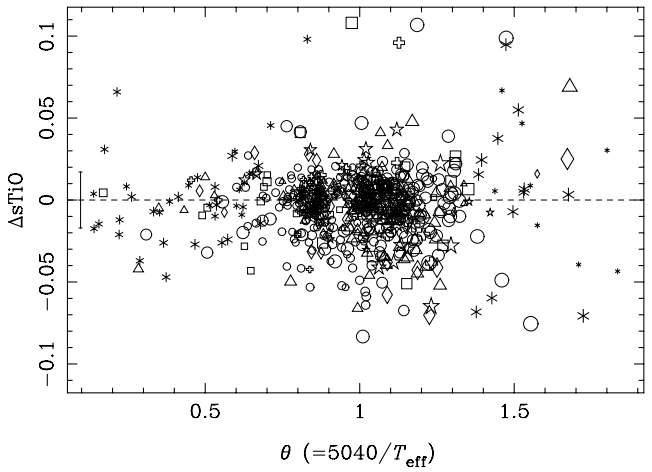

Figure 15. Residuals of the sTiO FFs (ΔsTiO = sTiO$_{obs}$ − sTiO$_{pred}$) versus θ for the whole stellar library [see Fig. 9(a) for symbol codes]. The error bar at the left-hand margin indicates the unbiased residual standard deviation of the fit. See text in Section 3.3 for a study on the different error sources driving the observed residuals.

Table 7. Statistical data for the general FFs of the indices MgI and sTiO. N: number of stars; σ_{std}: unbiased residual standard deviation; σ_{typ}: typical index error for the stars used in the fits; r^2: determination coefficient.

	N	σ_{std}	σ_{typ}	r^2
MgI	647	0.091	0.043	0.91
sTiO	668	0.017	0.004	0.97

FFs (e.g. a weak dependence on temperature leads to small index errors due to T_{eff} uncertainties) and the atmospheric parameter range (e.g. both hot and very cold stars have T_{eff} uncertainties larger than intermediate temperature stars), we have performed the analysis not only for the stellar library as a whole but also for different sets of stars (listed in Table 8).

For each star of the sample, we have derived three index errors, arising from the corresponding uncertainties in T_{eff}, $\log g$ and [Fe/H]. As input atmospheric parameter uncertainties, we have made use of the values presented in table 7 of CEN01b. Apart from those, we have used errors of 75 K, 0.40 dex and 0.15 dex for the effective temperatures, gravities and metallicities taken from Soubiran et al. (1998) (with 4000 K $< T_{eff} <$ 6300 K; stars coded SKC in table 6 of CEN01b), and 75 K, 0.05 dex and 0.20 dex for the cluster stars. For each subset of stars, we have computed a mean index error as a result of the uncertainty of each parameter ($\sigma_{T_{eff}}$, $\sigma_{\log g}$ and $\sigma_{[Fe/H]}$) by using the input parameter errors for all the individual stars. Finally, an estimate of the total expected error due to atmospheric parameters (σ_{par}) is computed as the quadratic addition of the three previous errors.

It is clear from the data in Table 8 that σ_{par} is, in all cases, comparable or larger than σ_{typ}. This result reinforces the importance of using a homogeneous and reliable set of atmospheric parameters to guarantee the accuracy of this kind of calibrations. Also, it is interesting to see how $\sigma_{T_{eff}}$ for cold stars is much larger than their observed dispersion w.r.t. the fits, σ_{std}. This would mean that the error in T_{eff} quoted in CEN01b for these types of stars was somewhat overestimated.

Furthermore, since the aim of this paper is to predict reliable index values for any combination of input atmospheric parameters, we have also computed the random errors in such predictions making use of the covariance matrices of the fits. These uncertainties are given in Table 9 for some representative values of input parameters. Note that as expected the absolute errors are larger for cold giants and supergiants and, in general, increase as the metallicity departs from the solar value. These errors are the ones provided by the FORTRAN routine that computes the FF predictions as uncertainties of the output MgI and sTiO indices.

3.3.2 *Uncertainties in the flux calibration*

An additional source of index errors that may increase the FF residuals is the uncertainty in the flux calibration of the library stars. At this point, we are not interested in the quality of the flux calibration in an absolute sense, as any minor departure from the 'true' calibration must be considered as a systematic that applies to the stellar library as a whole, and hence it would not affect the FF residuals. Instead, we aim at constraining the random errors in the final flux calibration curve and their effects on the index measurements.

It is important to note that, in CEN01a, all the stars of a given observing run were flux calibrated by applying one response curve, the one that was obtained as an average of all the individual response curves derived from single observations of spectrophotometric standard stars (10–20 per observing run). Therefore, using each of the above individual curves to re-calibrate the stellar spectra, we repeated the index measurements for all the stars to estimate a random error, arising from flux calibration uncertainties (σ_{fcal}), as the rms standard deviation of all the individual index measurements.

The above procedure allowed us to confirm that, as expected (see Section 2.4.3), and unlike MgI, sTiO is very sensitive to flux calibration. On average over all the different observing runs, we obtain that $\sigma_{fcal} \sim 0.012 \times$ sTiO, which turns the flux calibration uncertainty into the main source of random error of the index sTiO (much larger than the joint effect of photon noise and radial velocity uncertainty). With typical sTiO values in the range 0.90–0.95, the majority of hot and intermediate T_{eff} stars ($T_{eff} \gtrsim$ 3900 K; $\theta \lesssim$ 1.30 K^{-1}) have $\sigma_{fcal} \sim 0.011$. Colder stars, however, having a much larger sTiO values, reach errors of up to $\sigma_{fcal} \sim 0.031$. According to the averaged sTiO values of the distinct categories of stars, different σ_{fcal} values for sTiO are given in Table 8. In addition, a typical value of $\sigma_{fcal} = 0.007$ Å for MgI has been derived from all the library stars.

3.3.3 *Overall random uncertainties*

The quadratic addition of σ_{typ}, σ_{par} and σ_{fcal} can be interpreted as an overall random uncertainty, σ_{ALL}, which is computed and listed for each group of stars in Table 8. Note that, unlike what happens for σ_{typ}, the new σ_{ALL} values account for most of (or even all) the dispersion of the fits, σ_{std}. In other words, the residuals of the fits are consistent with the expected scatter due to the individual index errors. This is particularly true for sTiO, with $\sigma_{ALL} = 0.016$ and $\sigma_{std} = 0.017$ for the whole stellar library. However, it seems that an additional source of error is still needed to reconcile σ_{ALL} and σ_{std} for MgI. This point is addressed in more detail in Section 3.4.

3.4 [Mg/Fe] abundance ratios

Given that MgI is an Mg I index, in principle one would expect its metallicity dependence to be better described in terms of the Mg abundance, [Mg/H], rather than [Fe/H]. In this section, we constrain

Table 8. Uncertainties of the MgI and sTiO FFs for different subsets of stars, and mean index errors due to uncertainties in the flux calibration and the input atmospheric parameters. Open clusters are Coma, Hyades, M67, NGC 188 and NGC 7789. Globular clusters include M3, M5, M10, M13, M71, M92 and NGC 6171. N: number of stars. $\sigma_{\rm typ}$: typical observational index error, accounting for photon noise and typical uncertainties in radial velocity. $\sigma_{T_{\rm eff}}$, $\sigma_{\log g}$ and $\sigma_{\rm [Fe/H]}$: mean index errors due to uncertainties in the input $T_{\rm eff}$, $\log g$ and [Fe/H]. $\sigma_{\rm par}$: total error due to atmospheric parameters (quadratic addition of the three previous ones). $\sigma_{\rm fcal}$: mean index error arising from random uncertainties in the flux calibration. $\sigma_{\rm ALL}$: total error due to all the above uncertainties (quadratic addition of $\sigma_{\rm typ}$, $\sigma_{\rm par}$ and $\sigma_{\rm fcal}$). $\sigma_{\rm std}$: unbiased residual standard deviation of the fit.

	Index	N	$\sigma_{\rm typ}$	$\sigma_{T_{\rm eff}}$	$\sigma_{\log g}$	$\sigma_{\rm [Fe/H]}$	$\sigma_{\rm par}$	$\sigma_{\rm fcal}$	$\sigma_{\rm ALL}$	$\sigma_{\rm std}$
Open clusters	MgI	92	0.065	0.037	0.009	0.056	0.068	0.007	0.094	0.114
	sTiO	93	0.006	0.003	0.001	0.001	0.003	0.011	0.013	0.017
Globular clusters	MgI	53	0.174	0.019	0.006	0.056	0.060	0.007	0.184	0.219
	sTiO	54	0.015	0.002	0.002	0.003	0.004	0.011	0.019	0.028
Field dwarfs	MgI	236	0.042	0.030	0.029	0.026	0.049	0.007	0.065	0.082
	sTiO	242	0.004	0.004	0.003	0.001	0.005	0.012	0.014	0.011
Field giants	MgI	196	0.036	0.026	0.009	0.028	0.039	0.007	0.054	0.091
	sTiO	204	0.003	0.017	0.004	0.001	0.017	0.012	0.021	0.016
Field supergiants	MgI	70	0.039	0.030	0.025	0.030	0.049	0.007	0.063	0.092
	sTiO	75	0.004	0.023	0.007	0.002	0.024	0.012	0.027	0.031
Hot stars ($0.13 < \theta < 0.69$)	MgI	67	0.040	0.054	0.014	0.023	0.061	0.007	0.073	0.086
	sTiO	68	0.004	0.010	0.003	0.000	0.011	0.011	0.016	0.022
Intermediate stars ($0.69 < \theta < 1.30$)	MgI	555	0.044	0.023	0.018	0.036	0.047	0.007	0.065	0.090
	sTiO	560	0.004	0.001	0.003	0.001	0.004	0.012	0.013	0.016
Cold stars ($1.30 < \theta < 1.84$)	MgI	25	0.029	0.061	0.009	0.006	0.062	0.007	0.069	0.106
	sTiO	40	0.004	0.123	0.004	0.002	0.123	0.022	0.125	0.025
All	MgI	647	0.043	0.029	0.018	0.034	0.048	0.007	0.065	0.091
	sTiO	668	0.004	0.009	0.003	0.001	0.010	0.012	0.016	0.017

Table 9. Absolute errors in the FFs predictions for different values of the atmospheric parameters. Input $\log g$ values varying with effective temperature for dwarfs, giants and supergiants have been taken from Lang (1991). Since for extreme temperatures, the FFs do not depend on metallicity, no [Fe/H] value has been adopted for 15 000 and 3200 K. This is also the case for some values at 3500 K.

		Dwarfs		Giants		Supergiants	
$T_{\rm eff}$	[Fe/H]	ΔsTiO	ΔMgI	ΔsTiO	ΔMgI	ΔsTiO	ΔMgI
15 000		0.001	0.041	0.001	0.041	0.007	0.029
8000	+0.5	0.002	0.031	0.002	0.031	0.007	0.039
8000	0.0	0.002	0.029	0.002	0.031	0.007	0.039
8000	−1.0	0.003	0.034	0.002	0.034	0.007	0.042
8000	−2.0	0.003	0.082	0.003	0.080	0.007	0.082
6000	+0.5	0.003	0.023	0.004	0.023	0.006	0.033
6000	0.0	0.002	0.013	0.003	0.016	0.006	0.029
6000	−1.0	0.003	0.018	0.004	0.021	0.006	0.033
6000	−2.0	0.006	0.048	0.005	0.048	0.007	0.054
5000	+0.5	0.005	0.045	0.003	0.031	0.006	0.038
5000	0.0	0.004	0.031	0.002	0.016	0.005	0.028
5000	−1.0	0.004	0.032	0.003	0.022	0.005	0.029
5000	−2.0	0.007	0.048	0.005	0.038	0.007	0.039
4000	+0.5	0.006	0.063	0.005	0.064	0.009	0.078
4000	0.0	0.006	0.051	0.004	0.037	0.008	0.063
4000	−1.0	0.006	0.052	0.004	0.055	0.007	0.066
4000	−2.0	0.007	0.084	0.007	0.120	0.009	0.114
3500	+0.5	0.010	0.045	0.027	0.072	0.027	0.073
3500	0.0	0.010	0.044	0.027	0.067	0.027	0.068
3500	−1.0	0.010	0.046	0.027	0.080	0.027	0.081
3500	−2.0	0.010	0.050	0.027	0.104	0.027	0.103
3200		0.011	0.041	0.042	0.063	0.042	0.063

the importance of different [Mg/Fe] ratios on driving the strength of the MgI index.

To do this analysis, we have compiled [Mg/Fe] data from the literature for 196 library stars. Most data were taken from the catalogue of Borkova & Marsakov (2005), as they performed a previous compilation of [Mg/Fe] data in the literature and, then, corrected the different sources from systematics to end up with a homogeneous [Mg/Fe] system. In addition, for a few stars which were not

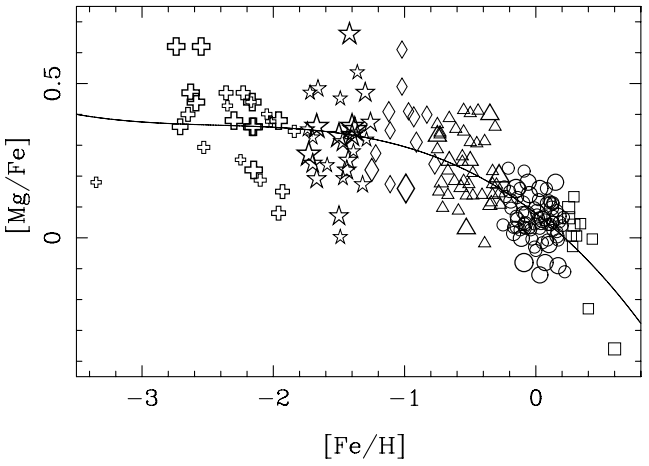

Figure 16. [Mg/Fe] abundance ratios versus [Fe/H] for 196 stars of the library in CEN01a. Different symbols and sizes indicate metallicities and gravities as in Fig. 9(a). The solid line is the least-squares fit to the data given in equation (10).

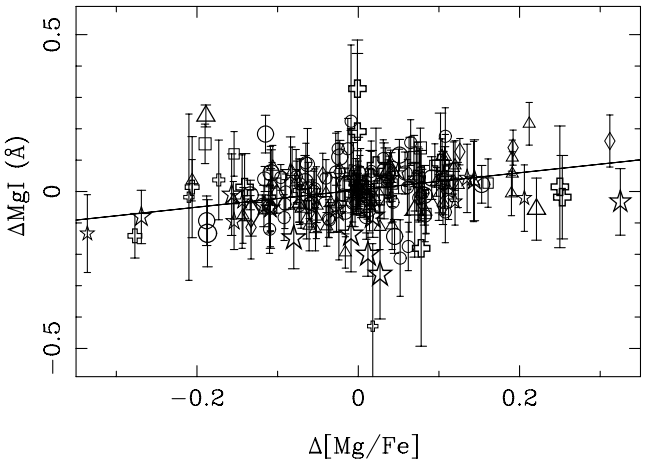

Figure 17. Residuals of the MgI FFs (ΔMgI; observed – predicted) versus residuals w.r.t. the intrinsic [Mg/Fe]–[Fe/H] relation of the stellar library (equation 10; Fig. 16). Symbols and sizes are as in Fig. 9(a). The solid line represents an error-weighted least-squares linear fit to all points within 3σ rms.

available in the above catalogue, we included the data from Gratton & Sneden (1987), Pilachowski, Sneden & Kraft (1996) and Thévenin (1998). The latter, having a large number of stars in common with Borkova & Marsakov, was previously transformed into Borkova & Marsakov's system by using all the stars in common between both catalogues.

Since our stellar library mainly consists of nearby stars, it matches the well-known [Mg/Fe]–[Fe/H] pattern of the solar neighbourhood (e.g. Edvardsson et al. 1993), in the sense that [Mg/Fe] decreases with the increasing [Fe/H]. Fig. 16 illustrates such a trend for the 196 library stars with available data. Far from being well represented by just a linear relationship, a least-squares polynomial fit to all the stars in Fig. 16 gives

$$[\mathrm{Mg/Fe}]_0 = 0.08(\pm0.01) - 0.33(\pm0.04)\,[\mathrm{Fe/H}] - 0.13(\pm0.04)\,[\mathrm{Fe/H}]^2 - 0.02(\pm0.01)\,[\mathrm{Fe/H}]^3, \quad (10)$$

where $[\mathrm{Mg/Fe}]_0$ can be considered the averaged [Mg/Fe] ratio of the solar neighbourhood. Note that such a relationship is implicitly taken into account in the FFs through the adopted [Fe/H], and therefore a systematic trend between the MgI FF residuals and the [Mg/Fe] ratios should not be expected. We have therefore investigated whether the residuals of the MgI FFs for individual stars (ΔMgI; as defined in Section 3.3) are correlated with their deviations from equation (10) ($\Delta[\mathrm{Mg/Fe}] \equiv [\mathrm{Mg/Fe}] - [\mathrm{Mg/Fe}]_0$). Fig. 17 confirms that there is indeed a significant relation between ΔMgI and Δ[Mg/Fe], in the sense that stars with larger Mg abundances (at fixed [Fe/H]) tend to have positive residuals in the MgI FFs. An error-weighted linear fit to this trend gives

$$\Delta\mathrm{MgI} = 0.005(\pm0.006) + 0.27(\pm0.09)\Delta[\mathrm{Mg/Fe}]. \quad (11)$$

An immediate implication of the above correlation is that it must account for part of the *unexplained* MgI residuals reported in Section 3.3.3. In fact, the variance of the fit in equation (11) is approximately 10 per cent smaller than σ^2_{std} of MgI for the stars in Fig. 17. If this subsample were representative of the whole library, different [Mg/Fe] ratios might explain ∼0.029 Å of the total MgI σ_{std} (0.091 Å). As a matter of fact, this number must be considered as a lower limit since cluster stars do not necessarily follow the [Mg/Fe] pattern of field stars (see Section 3.4.1) and larger MgI residuals are expected for this subsample of stars. In addition, the existence of the correlation given in equation (11) demonstrates that the MgI index is indeed a good indicator of the Mg abundance. Note that this is not necessarily true for all metal-line indices, as it was demonstrated in CEN02 that the Ca II triplet indices do not depend on minor changes in [Ca/Fe].

Unfortunately, [Mg/Fe] ratios are only available for less than one-third of the library stars. Even though this number is large enough to perform a reliable analysis as the one presented above, it is not worth trying to include an [Mg/Fe] term in our FFs, as not only the small number of stars but also the more limited atmospheric parameter coverage of the subsample would dramatically affect the accuracy and reliability of the empirical calibration. Instead, we prefer to keep the FFs in their present form and stress the idea that, by being constrained to the chemical enrichment of the solar neighbourhood, they are subject to exhibit systematics with respect to other enrichment scenarios in which Mg abundances are well different.

3.4.1 The MgI residual of M67

Compared to the predictions of the MgI FFs, M67 stars show a significant mean offset of $\Delta\mathrm{MgI} = -0.134 \pm 0.022$ Å that cannot be solely explained by typical random errors. Fig. 18 illustrates the derived offsets for all the 20 stars in M67.

Given that the sensitivity of MgI to $\log g$ is relatively small as compared to other atmospheric parameters, small uncertainties in the distance moduli adopted by the original references that derived surface gravities (see CEN01b) are not expected to be responsible for the observed discrepancy. Instead, since MgI increases with metallicity, the negative MgI residual of M67 could be explained if the true cluster metallicity were lower than the value adopted in this work ([Fe/H] = −0.09, from Friel & Janes 1993; see CEN01b). In this sense, according to our FF predictions, a cluster metallicity of [Fe/H] ∼ −0.32 would suffice to make the offset statistically non-significant given the MgI errors of the M67 stars. However, apart from the pioneering work by Cohen (1980) in which an averaged value of [Fe/H] = −0.39 was reported for M67, more recent work derived roughly solar (or slightly below solar) iron abundances for the cluster stars, like, e.g., −0.1 ± 0.1 (Foy & Proust 1981), −0.09 ± 0.07 (Friel & Janes 1993), −0.15 ± 0.05 (Friel et al.

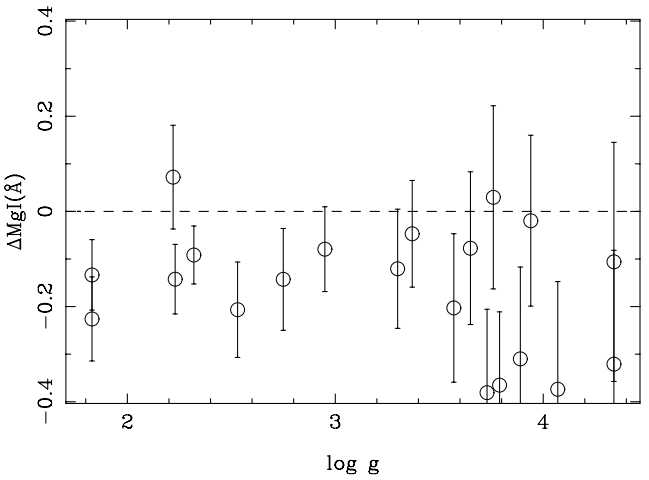

Figure 18. MgI residuals (ΔMgI; observed – predicted) versus log g for M67 stars. A significant offset of $\Delta\mathrm{MgI} = -0.134 \pm 0.022$ Å is observed.

2002), -0.03 ± 0.03 (Tautvaišiene et al. 2000), $+0.02 \pm 0.06$ (Gratton 2000). Therefore, assuming that the adopted value is a reasonable compromise for the [Fe/H] of the cluster, and keeping in mind that MgI indeed depends on the Mg abundance, the MgI residual could be a natural consequence of [Mg/Fe] differences between M67 stars and field stars at similar [Fe/H].

With regard to the [Mg/Fe] value of M67, there seems to exist some discrepancy in the literature. For instance, Tautvaišiene et al. (2000) reported [Mg/Fe] $\sim +0.1$ for evolved (giant and clump) stars in M67, whilst an error-weighted mean of the values presented by Shetrone & Sandquist (2000) for a sample of turn-off stars and blue stragglers in the cluster gives $[\mathrm{Mg/Fe}] = -0.14 \pm 0.10$.

Making use of equation (10), it is easy to convert [Fe/H] into [Mg/H] abundances to test the above hypothesis. At $[\mathrm{Fe/H}] = -0.09$ (the metallicity adopted for M67), field library stars have an average value of $[\mathrm{Mg/H}] = +0.02$ ($[\mathrm{Mg/Fe}] = +0.11$), whereas at $[\mathrm{Fe/H}] = -0.32$ (the value at which the MgI residual would not be significant), $[\mathrm{Mg/H}] = -0.13$ ($[\mathrm{Mg/Fe}] = +0.19$). This implies that, if MgI is indeed driven by Mg rather than Fe, the MgI residual of M67 could be explained if the Mg content of its stars were offset by $\Delta[\mathrm{Mg/H}] = -0.15$ with respect to that of field stars. In other words, keeping $[\mathrm{Fe/H}] = -0.09$ for M67, a value of [Mg/Fe] ~ -0.04 for M67 is required to account for the MgI residuals. This value is in good agreement with the work by Schiavon, Caldwell & Rose (2004), which constrains the [Mg/Fe] of M67 between -0.1 and 0.0 on the basis of the integrated Mg*b* in the cluster spectrum. Also, it is consistent with previous result from Friel & Janes (1993) that the metallicity derived for M67 from Mg*b* is significantly lower than the one inferred from Fe indices. We therefore conclude that the MgI residual of M67 is probably driven by the existence of an Mg underabundance of [Mg/Fe] ~ -0.04, in contrast with the averaged value [Mg/Fe] $\sim +0.11$ for field library stars of equal [Fe/H].

4 A COMPARISON WITH THEORETICAL WORK

We provide here a qualitative comparison between the new FFs presented in this paper and the MgI and sTiO predictions derived from theoretical work based on model atmospheres, in particular from the high-resolution synthetic stellar spectral library of Coelho et al. (2005, hereafter C05). This theoretical library ranges from the near-ultraviolet to the near-IR, spanning the atmospheric parameter range of $3500 \leq T_{\rm eff} \leq 7000$ K, $0.0 \leq \log g \leq 5.0$ dex, and $-2.5 \leq [\mathrm{Fe/H}] \leq +0.5$ dex, at two different α-element abundance ratios, $[\alpha/\mathrm{Fe}] = 0.0$ and $+0.4$.

Prior to measuring the MgI and sTiO indices over the C05 stellar spectra, we smoothed and rebinned the C05 stellar spectra to match the spectral resolution and linear dispersion of the stars in CEN01a (FWHM = 1.5 Å; 0.85 Å pixel^{-1}). Also, for the sake of carrying out a meaningful comparison with our predictions, we removed from the current analysis all those synthetic stars that, because of their atmospheric parameters, are not expected to be required by SSP codes. This includes, for instance, late spectral types with intermediate surface gravity values (e.g. from $T_{\rm eff} = 4500$ K and $\log g = 4$ dex, down to $T_{\rm eff} = 3500$ K and $1.5 \leq \log g \leq 4$ dex), and hot dwarfs with very high surface gravity values ($T_{\rm eff} \geq 5000$ K and $\log g = 5$). This way, we also guaranteed that the overall atmospheric parameter space of the synthetic stars is not very different from that covered by the real stars in CEN01a.

To avoid systematics between the MgI of both samples arising from the existence of different Mg abundances at fixed [Fe/H], we took into account the [Mg/Fe]–[Fe/H] abundance pattern of the stars in CEN01a (see Section 3.4) and corrected the C05 indices for this effect. To do this, for each [Fe/H] value in C05 we determined its corresponding [Mg/Fe] according to equation (10). Hence, the final MgI and sTiO indices for the synthetic C05 stellar spectra are the result of interpolating linearly the indices measured at $[\alpha/\mathrm{Fe}] = 0.0$ and 0.4 according to the above [Mg/Fe] value.

With all the considerations given above, the four left-hand panels in Fig. 19 illustrate a comparison between the MgI and sTiO indices measured on the C05 synthetic stars and those derived from our MgI and sTiO FFs for exactly the same atmospheric parameters of the synthetic stars. Although there exists a reasonable qualitative agreement in the first-order behaviours of both data sets, absolute numbers reveal significant differences between real and synthetic indices. This is more clearly presented in the four right-hand panels of Fig. 19, where the star-by-star absolute differences are plotted versus θ and $\log g$. The rms standard deviation of the index differences is $\sigma_{\rm std} = 0.142$ Å and 0.042 for MgI and sTiO, respectively, much larger than the typical residuals in Table 7 and Figs 14 and 15. Some of these differences may be due to the limitation of our FFs to reproduce the poorly populated regions of the parameter space (e.g. the MgI of metal-poor stars at $\theta \sim 1.2$; see discussion in Section 3.2.2). However, most cases cannot be justified in this way (e.g. synthetic MgI and sTiO indices do not reproduce satisfactorily the gravity dependence exhibited by real stars, particularly for intermediate-to-high metallicity giants) and the intrinsic limitations of theoretical model atmospheres hence appear as potential sources for the observed differences. It is not, however, the scope of this section to provide a detailed analysis of the origins for the observed differences but to illustrate the reader with a comparative analysis between theoretical and empirical work. A similar comparison for the Ca II triplet lines can be found in VAZ03.

5 SUMMARY AND CONCLUSIONS

Based on the near-IR stellar library of CEN01a and CEN01b, we have defined new line-strength indices for the Mg I line at 8807 Å and the TiO bands around the Ca II triplet region. These indices, called MgI and sTiO, respectively, are thought to be used as stellar population diagnostics. For this reason, we have characterized their sensitivities to different S/N, distinct spectral resolutions, flux

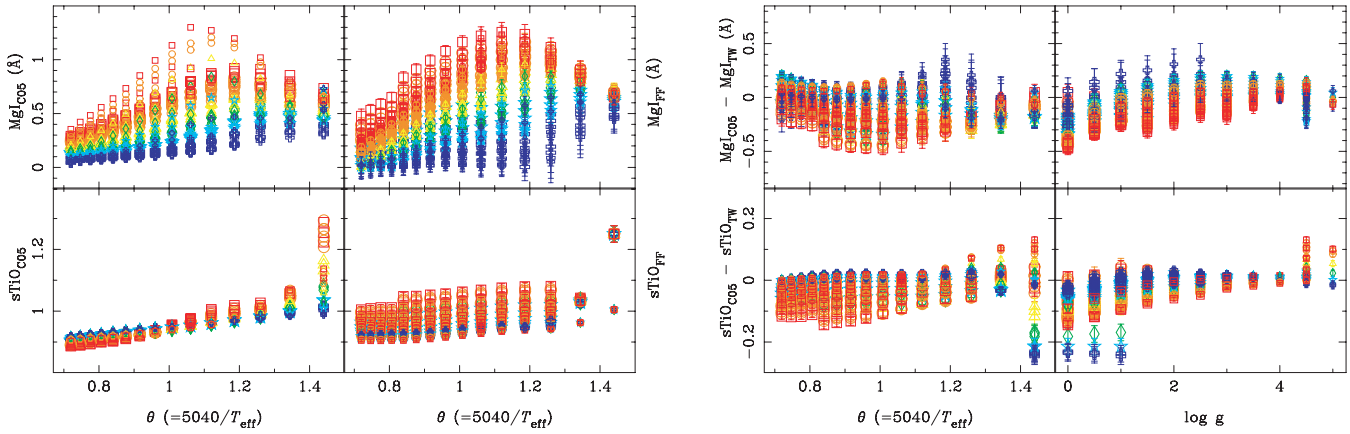

Figure 19. Left four panels: a comparison between the MgI and sTiO indices measured for the synthetic stars of C05 and those predicted by the FFs of this paper at exactly the same atmospheric parameters of the synthetic stars. Right four panels: star-by-star differences between the C05 and FF indices versus θ and log g. For each index, vertical scales have been set to the same relative ranges of left-hand panels to allow direct comparisons. Symbol types and relative sizes (indicating, respectively, metallicity and gravity ranges) are as given in Fig. 9(a). See more details given in the text.

calibration and reddening correction systematics, and the presence of sky line residuals typical of this spectral range. Also, we give some recipes for those readers interested in transforming their old MgI and TiO index data into our new system of indices.

After measuring MgI and sTiO for all the library stars at the spectral resolution of CEN01a, we have calibrated their dependences on the stellar atmospheric parameters ($T_{\rm eff}$, log g and [Fe/H]) by means of empirical FFs. The reliability and accuracy of the new FF predictions have been discussed by performing a thorough analysis of the different error sources driving the FF residuals. For sTiO, these residuals are overall compatible with the ones expected from the uncertainties in the input atmospheric parameters and from the random errors in the index measurements (accounting for photon noise, radial velocity uncertainties and flux calibration errors). For MgI, however, an additional contribution to the FF residuals arises from the existence of distinct [Mg/Fe] ratios among the library stars. As a consequence of this analysis, we have detected a statistically significant offset in the MgI values of M67 stars. This is consistent with M67 having an [Mg/Fe] underabundance of ~ -0.04, in contrast with the typical [Mg/Fe] $\sim +0.11$ of solar-neighbourhood stars with the same [Fe/H].

A full data base with the index measurements for each library star, their random errors, the FF residuals and the compiled [Mg/Fe] values is given in Table 10. [A sample of Table 10 is included here; the full table is available in the online version of the article (see Supporting Information).] This data base, together with the FORTRAN routine for the evaluation of the FFs, is also available at http://www.ucm.es/info/Astrof/ellipt/MgIsTiO.html. In a forthcoming paper (Vazdekis et al. in preparation), SSP model predictions for MgI and sTiO will be presented on the basis of such FFs, either at the above website and at A. Vazdekis models website.[2]

To conclude, a brief summary of the main characteristics of the indices, their behaviours and their potential capabilities for stellar population studies is given below.

(i) MgI has been specifically designed to be a very sensitive indicator of Mg abundance. For this reason, because of its relatively narrow line bandpass, it turns out to be dependent on the overall spectral resolution (and, hence, on the velocity dispersion of galaxies). Users are therefore encouraged to put their data into a homogeneous system of spectral resolution (either using the sigma-dependent polynomials provided in Table 3, or broadening their spectra up to a common overall spectral resolution) before any meaningful comparison of the MgI index among different types of objects.

MgI exhibits a complex dependence on the three main stellar atmospheric parameters. For hot and cold stars, $T_{\rm eff}$ and log g are the main driving parameters, whereas, in the mid-temperature regime ($4000 \leq T_{\rm eff} \leq 7000$ K), all three parameters play a significant role: MgI increases with the increasing metallicity and the decreasing temperature, with a mild dependence on the luminosity class that makes dwarfs and supergiant stars to exhibit slightly larger MgI values than giant stars.

For stellar population studies, as it will be shown in a forthcoming paper (Vazdekis et al., in preparation), the integrated MgI turns out to be an excellent indicator of the Mg abundance.

(ii) The sTiO index has been defined to measure the slope of the pseudo-continuum of the Ca II triplet region, which is known to change dramatically for M-type stars due to the appearance of strong TiO molecular bands. Because of its definition, the sTiO index is strikingly robust against changes in spectral resolution – and velocity dispersions – and low S/N, which makes it particularly suited for the analysis of galaxies at high redshifts and extragalactic globular clusters. It, however, requires the spectra to have a proper relative flux calibration.

With regard to the behaviour of sTiO in stars, the steep increase with the decreasing temperature for $T_{\rm eff} \leq 3600$ K is worth noting. In turn, at such low temperatures, giant stars exhibit much stronger sTiO values than dwarfs, which makes sTiO a powerful dwarf-to-giant discriminator for M-type stars. In addition, the dependence of sTiO on the stellar metallicity is almost negligible.

For the integrated spectra of quiescent galaxies, however, sTiO is found to reflect the overall metallicity of the stellar population, as the red giant branch gets cooler with the increasing metallicity and the relative contribution of M-type stars increases (see VAZ03).

In Cenarro et al. (2003), both MgI and sTiO were measured for the first time over a sample of 35 elliptical galaxies, illustrating the usefulness of the MgI index to reproduce the Mg–σ relation of elliptical galaxies at the near-IR, and the capabilities of sTiO as metallicity indicator.

[2] http://www.iac.es/galeria/vazdekis/vazdekis_models.html

Table 10. MgI and sTiO index measurements ($\mathcal{I}$), typical observational index error ($\sigma_{\rm typ}\mathcal{I}$, accounting for photon noise and typical uncertainties in radial velocity), FF residuals ($\Delta\mathcal{I}$) and [Mg/Fe] abundances (when available) for all the stars in CEN01a. Sources for [Mg/Fe] values are: (1) the catalogue of spectroscopic abundances in stars (Borkova & Marsakov 2005); (2) the catalogue of chemical abundances in late-type stars (Thévenin 1998) corrected to the Borkova & Marsakov (2005) system; (3) Pilachowski et al. (1996) and (4) Gratton & Sneden (1987). The first five columns indicate the star number within the library, the name, the coordinates (RA and Dec. in J2000, except M71 stars which are B1950) and the spectral type and luminosity class. Additional information for the library stars (e.g. atmospheric parameters, [Ca/Fe] abundances, CaT, PaT and CaT* index values, their errors and FF residuals, *B* and *V* apparent magnitudes, S/N per angstrom and other names) can be found at CEN01a and CEN01b and at http://www.ucm.es/info/Astrof/ellipt/MgIsTiO.html. This is a sample of the full table, which is available in the online version of the article (see Supporting Information).

Num	Name	RA (h:m:s)	Dec. (d:m:s)	SpT	MgI(Å) $\mathcal{I}$	MgI(Å) $\sigma_{\rm typ}\mathcal{I}$	MgI(Å) $\Delta\mathcal{I}$	sTiO $\mathcal{I}$	sTiO $\sigma_{\rm typ}\mathcal{I}$	sTiO $\Delta\mathcal{I}$	[Mg/Fe]
001	Coma A 3	12:19:16.7	+25:26:11	G9 V	0.417	0.097	−0.430	0.900	0.008	−0.025	
002	Coma A 13	12:24:06.2	+26:07:44	K0 V	0.388	0.135	−0.318	0.865	0.010	−0.053	
003	Coma A 14	12:24:17.6	+24:19:32	G4 V	0.396	0.080	−0.297	0.920	0.007	−0.002	
004	Coma A 21	12:30:14.8	+25:01:44	G7 V	0.570	0.099	−0.185	0.919	0.008	−0.005	
005	Coma T 65	12:19:28.3	+24:17:03	G0 V	0.285	0.079	−0.143	0.896	0.006	−0.017	
006	Coma T 68	12:19:50.6	+28:27:51	A6 IV-V	−0.064	0.066	−0.008	0.920	0.005	−0.016	
007	Coma T 82	12:21:26.7	+24:59:49	A9 V	−0.214	0.072	−0.257	0.893	0.005	−0.025	
008	Coma T 85	12:21:49.0	+26:32:57	G1 V	0.487	0.062	0.049	0.904	0.005	−0.008	
009	Coma T 86	12:21:56.2	+27:18:34	F6 V	0.068	0.071	−0.202	0.888	0.006	−0.024	
010	Coma T 90	12:22:24.8	+22:27:51	F5 V	0.100	0.071	−0.183	0.886	0.006	−0.026	
011	Coma T 97	12:23:08.4	+25:51:05	F9 V	0.462	0.084	0.068	0.906	0.007	−0.006	
012	Coma T 102	12:23:42.2	+26:36:08	G1 V	0.338	0.122	−0.123	0.896	0.010	−0.017	
013	Coma T 114	12:25:22.5	+23:13:45	F8 V	0.297	0.073	0.037	0.892	0.006	−0.019	
014	Coma T 132	12:27:06.1	+26:50:47	G5 V	0.598	0.096	0.017	0.877	0.008	−0.037	
015	Coma T 150	12:29:41.1	+24:31:13	G9 V	0.465	0.080	−0.213	0.889	0.006	−0.033	

ACKNOWLEDGMENTS

We acknowledge an anonymous referee for his/her very useful comments. AJC is a *Juan de la Cierva* Fellow of the Spanish Ministry of Science and Innovation. This work has been funded by the Spanish Ministry of Science and Innovation through grants AYA2007-67752-C03-01 and AYA2006-15698-C02-02.

REFERENCES

Borkova T. V., Marsakov V. A., 2005, Astron. Rep., 49, 405
Bruzual G., Charlot S., 2003, MNRAS, 344, 1000
Cardiel N., 2007, in Figueras F., Girart J. M., Hernanz M., Jordi C., eds, Highlights of Spanish Astrophysics IV, Proceedings of the 7th Scientific Meeting of the Spanish Astronomical Society. CDROM. Springer, Berlin
Cardiel N., Gorgas J., Cenarro J., Gonzalez J. J., 1998, A&AS, 127, 597
Carter D., Visvanathan N., Pickles A. J., 1986, ApJ, 311, 637 (CVP)
Cenarro A. J., Cardiel N., Gorgas J., Peletier R. F., Vazdekis A., Prada F., 2001a, MNRAS, 326, 959 (CEN01a)
Cenarro A. J., Gorgas J., Cardiel N., Vazdekis A., Prada F., 2001b, yCat, 832, 60959
Cenarro A. J., Gorgas J., Cardiel N., Pedraz S., Peletier R. F., Vazdekis A., 2001b, MNRAS, 326, 981 (CEN01b)
Cenarro A. J., Gorgas J., Cardiel N., Vazdekis A., Peletier R. F., 2002, MNRAS, 329, 863 (CEN02)
Cenarro A. J., Gorgas J., Vazdekis A., Cardiel N., Peletier R. F., 2003, MNRAS, 339, L12
Cenarro A. J. et al., 2007, MNRAS, 374, 664
Chmielewski Y., 2000, A&A, 353, 666
Cid Fernandes R., Mateus A., Sodré L., Stasińska G., Gomes J. M., 2005, MNRAS, 358, 363
Coelho P., Barbuy B., Meléndez J., Schiavon R. P., Castilho B. V., 2005, A&A, 443, 735 (C05)
Cohen J. G., 1980, ApJ, 241, 981
Díaz A. I., Terlevich E., Terlevich R., 1989, MNRAS, 239, 325 (DTT)
Dressler A., Lynden-Bell D., Burstein D., Davies R. L., Faber S. M., Terlevich R., Wegner G., 1987, ApJ, 313, 42
Edvardsson B., Andersen J., Gustafsson B., Lambert D. L., Nissen P. E., Tomkin J., 1993, A&A, 275, 101
Fanelli M. N., O'Connell R. W., Burstein D., Wu C.-C., 1992, ApJS, 82, 197
Fitzpatrick E. L., 1999, PASP, 111, 63
Foy R., Proust D., 1981, A&A, 99, 221
Friel E. D., Janes K. A., 1993, A&A, 267, 75
Friel E. D., Janes K. A., Tavarez M., Scott J., Katsanis R., Lotz J., Hong L., Miller N., 2002, AJ, 124, 2693
Gilbert K. M. et al., 2006, ApJ, 652, 1188
Gorgas J., Faber S. M., Burstein D., Gonzalez J. J., Courteau S., Prosser C., 1993, ApJS, 86, 153
Gorgas J., Cardiel N., Pedraz S., González J. J., 1999, A&AS, 139, 29
Gratton R., 2000, in Pallavicini R., Micela G. and Sciortino S., eds, ASP Conf. Ser. Vol. 198. Stellar Clusters and Associations: Convection, Rotation and Dynamos. Astron. Soc. Pac, San Francisco, p. 225
Gratton R. G., Sneden C., 1987, A&A, 178, 179
Gregg M. D. et al., 2004, A&AS, 36, 1496
Heap S. R., Lindler D. J., 2007, in Vallenari A., Tantalo R., Portinari L., eds, From Stars to Galaxies, ASP Conf. Ser. Vol. 374. Astron. Soc. Pac., San Francisco, p. 409
Ivanov V. D., Rieke M. J., Engelbracht C. W., Alonso-Herrero A., Rieke G. H., Luhman K. L., 2004, ApJS, 151, 387
Jones L. A., 1998, PhD thesis, Univ. North Carolina
Koleva M., Prugniel P., Ocvirk P., Le Borgne D., Soubiran C., 2008, MNRAS, 385, 1998
Lang K. R., 1991, Astrophysical Data: Planets and Stars. Springer-Verlag, Berlin
Le Borgne J.-F. et al., 2003, A&A, 402, 433
Le Borgne D., Rocca-Volmerange B., Prugniel P., Lançon A., Fioc M., Soubiran C., 2004, A&A, 425, 881
Maraston C., 2005, MNRAS, 362, 799
Maraston C., Nieves Colmenávez L., Bender R., Thomas D., 2009, A&A, 493, 425
Mármol-Queraltó E., Cardiel N., Cenarro A. J., Vazdekis A., Gorgas J., Pedraz S., Peletier R. F., Sánchez-Blázquez P., 2008, A&A, 489, 885

Mathis H., Charlot S., Brinchmann J., 2006, MNRAS, 365, 385
Ocvirk P., Pichon C., Lançon A., Thiébaut E., 2006a, MNRAS, 365, 46
Ocvirk P., Pichon C., Lançon A., Thiébaut E., 2006b, MNRAS, 365, 74
Panter B., Heavens A. F., Jimenez R., 2003, MNRAS, 343, 1145
Panter B., Jimenez R., Heavens A. F., Charlot S., 2007, MNRAS, 378, 1550
Pilachowski C. A., Sneden C., Kraft R. P., 1996, AJ, 111, 1689
Prugniel P., Soubiran C., 2001, A&A, 369, 1048
Prugniel P., Soubiran C., 2004, preprint (arXiv:astro-ph/0409214)
Prugniel P., Soubiran C., Koleva M., Le Borgne D., 2007, preprint (arXiv:astro-ph/0703658)
Ranade A., Gupta R., Ashok N. M., Singh H. P., 2004, Bull. Astron. Soc. India, 32, 311
Ranade A. C., Singh H. P., Gupta R., Ashok N. M., 2007a, Bull. Astron. Soc. India, 35, 87
Ranade A. C., Ashok N. M., Singh H. P., Gupta R., 2007b, Bull. Astron. Soc. India, 35, 359
Rousselot P., Lidman C., Cuby J.-G., Moreels G., Monnet G., 2000, A&A, 354, 1134
Sánchez-Blázquez P. et al., 2006, MNRAS, 371, 703
Schiavon R. P., 2007, ApJS, 171, 146
Schiavon R. P., Caldwell N., Rose J. A., 2004, AJ, 127, 1513
Shetrone M. D., Sandquist E. L., 2000, AJ, 120, 1913
Soubiran C., Katz D., Cayrel R., 1998, A&AS, 133, 221
Stevenson C. C., 1994, MNRAS, 267, 904
Tautvaišiene G., Edvardsson B., Tuominen I., Ilyin I., 2000, A&A, 360, 499
Thévenin F., 1998, yCat, 3193, 0
Thomas D., Maraston C., Bender R., 2003, MNRAS, 339, 897
Valdés F., Gupta R., Rose J. A., Singh H. P., Bell D. J., 2004, ApJS, 152, 251
Vazdekis A., 1999, ApJ, 513, 224
Vazdekis A., Casuso E., Peletier R. F., Beckman J. E., 1996, ApJS, 106, 307
Vazdekis A., Cenarro A. J., Gorgas J., Cardiel N., Peletier R. F., 2003, MNRAS, 340, 1317 (VAZ03)
Worthey G., 1994, ApJS, 95, 107
Worthey G., Ottaviani D. L., 1997, ApJS, 111, 377
Worthey G., Faber S. M., Gonzalez J. J., 1992, ApJ, 398, 69
Worthey G., Faber S. M., Gonzalez J. J., Burstein D., 1994, ApJS, 94, 687

SUPPORTING INFORMATION

Additional Supporting Information may be found in the online version of this article.

Table 10. MgI and sTiO index measurements ($\mathcal{I}$), typical observational index error ($\sigma_{\rm typ}\mathcal{I}$, accounting for photon noise and typical uncertainties in radial velocity), FF residuals ($\Delta\mathcal{I}$) and [Mg/Fe] abundances (when available) for all the stars in CEN01a.

Please note: Wiley-Blackwell are not responsible for the content or functionality of any supporting materials supplied by the authors. Any queries (other than missing material) should be directed to the corresponding author for the article.

This paper has been typeset from a TEX/LATEX file prepared by the author.